Soft genome editing based on CRISPR nickases: it takes one break to tango

Wang, Q.

Chapter 7

The chromatin context differently impacts prime editors and base editors and further controls the fidelity and purity of base editing

Qian Wang[1,†], Hidde Zittersteijn[1,†], Xiaoling Wang[1], Josephine M. Janssen[1], Jin Liu[1], Leon Mei[2], Rob C. Hoeben[1] and Manuel A.F.V. Gonçalves[1]

[1]Department of Cell and Chemical Biology, Leiden University Medical Center, Einthovenweg 20, 2333 ZC Leiden, the Netherlands;
[2]Department of Biomedical Data Sciences, Sequencing Analysis Support Core, Leiden University Medical Center, Einthovenweg 20, 2333 ZC Leiden, the Netherlands
[†]These authors contributed equally

Under revision at Molecular Cell

ABSTRACT

Base editors and prime editors allow changing specific nucleotide sequences within the vast genomes of eukaryotic cells requiring neither mutagenic double-stranded DNA breaks nor exogenous donor DNA substrates. However, the performance of base editors vis-à-vis prime editors at alternate chromatin states is ill-defined. Moreover, the role of the chromatin environment of target sequences and its underlying factors on DNA editing product fidelity and purity is equally unknown. Here, using cellular systems that permit assessing the efficiency and fidelity of gene-editing tools at isogenic target sequences controlled by specific epigenetic factors, we report that heterochromatin impinged by the KRAB/KAP-1/HP1 axis alone or together with the DNA methyltransferases DNMT3A and DNMT3L, mostly hinders prime editors over base editors with the extended portions of prime-editing guide RNAs contributing to this outcome. Indeed, the performance of base editors at heterochromatin ranges in a target site-dependent manner from lower to, often, significantly higher than that observed at euchromatin. Additionally, the extent and types of byproducts accumulated after base editing is also contingent upon the epigenetic context of target sequences. Our findings have direct implications for the optimal assessment of these powerful genomic engineering tools and might guide their selection, further development and application.

INTRODUCTION

Genome editing based on CRISPR-associated (Cas) nucleases and sequence-customizable single guide RNAs (gRNAs) has become a powerful approach for introducing specific genetic changes (edits) in living cells[1]. However, in addition to the intended edits, repair of double-stranded DNA breaks (DSBs) by error-prone recombination processes frequently yields unwanted byproducts in the form of uncontrolled insertions and deletions (indels)[2-5], genome-wide translocations[6-10] and gross on-target chromosomal rearrangements[6,11]. Recent studies have also uncovered loss-of-heterozygosity, chromosome fragmentation followed by haphazard DNA reassembly (chromothripsis)**,** and whole chromosome losses (aneuploidy) upon target DSB formation[12-14]. Thus, although emerging high-specificity nucleases present reduced off-target activities[1,15,16], they are inherently incapable of eliminating the unintended and poorly controlled effects resulting from on-target DSBs. Therefore, increasing research is directed to substituting programmable nucleases by DSB-free genome editing systems, such as those based on Cas9 nickases as such[17-20], or on these nickases fused to DNA modifying effector domains that form base editors[21-24] and, more recently, prime editors[25].

Base editing complexes comprise a conventional gRNA and a Cas9^{D10A} nickase (**Supplementary Figure S1**) fused to cytidine or adenine deaminases[21-24]. Deaminated nucleotides generated *in situ* by cytidine base editors (CBEs) and adenine base editors (ABEs) are processed through DNA repair mechanisms ultimately yielding C•G-to-T•A (C→T) and A•T-to-G•C (A→G) transitions, respectively (**Supplementary Figure S1**). These base-pair substitutions take place prevalently within a so-called "editing window" whose length and location in the gRNA target sequence (protospacer) depends on the particular base editor architecture[24].

Prime editing complexes consist of an extended gRNA, named pegRNA, and a Cas9^{H840A} nickase fused to an engineered reverse transcriptase (RT) (**Supplementary Figure S2**). The pegRNA is formed by a gRNA covalently linked to RT template and primer binding site (PBS) sequences. Targeted nicking by Cas9^{H840A} releases a DNA flap that, upon annealing to the PBS, primes reverse transcription over the RT template that encodes the edit-of-interest. Through a series of cellular processing steps, the resulting DNA copy becomes ultimately incorporated at the genomic target site (**Supplementary Figure S2**). Although detailed investigation on the late-stage processing steps is required, DNA mismatch repair factors and cellular replication were recently shown to be determinants of prime editing[26-28]. Prime editing has two generic modalities, namely, PE2 and PE3. The former system relies exclusively on PE2:pegRNA complexes; the latter depends on the concerted action of PE2:pegRNA and PE2:gRNA complexes (**Supplementary Figure S2**). The PE3 system has enhanced activity, although the nicking of both DNA strands by PE3 components can foster indel byproduct accumulation[25].

Base editors are restricted to installing specific base-pair substitutions, whilst prime editors install well-defined insertions and deletions in addition to all 12 base-pair substitutions and combinations thereof[25]. Moreover, CBE and ABE deaminase effectors often do not discriminate target from nearby non-target nucleotides and can install unintended substitutions leading to reduced product purity[24]. Conversely,

base editors yield low indel byproducts and are normally more robust than prime editors at randomly selected target sequences. Hence, base editors and prime editors present a rather complementary set of attributes in terms of their editing versatility, robustness, and fidelity. It is, therefore, essential to identify the parameters underlying the individual and relative performances of base editors and primer editors to guide their further development and selection to specific contexts and goals.

Research from our laboratory and that from others has demonstrated that the activity of different types of nucleases, including CRISPR-derived nucleases, are significantly hindered by heterochromatic states in living cells[29-32]. However, cause-effect associations between alternate chromatin conformations and the activity and fidelity of DSB-free genome editing platforms remain to be characterized and thoroughly assessed. Hence, in this work, we sought to address these knowledge gaps by implementing complementary loss-of-function and gain-of-function cellular systems in which isogenic target sequences acquire specific euchromatic and heterochromatic statuses through the controlled recruitment of endogenous epigenetic remodelling complexes. We report that primer editing is frequently hindered at Krüppel-associated box (KRAB)-impinged facultative heterochromatin as well as at heritable heterochromatin created by the concerted action of KRAB-recruited remodelling complexes and DNA methyltransferases (i.e., DNMT3A and DNMT3L). Moreover, we found that the underperformance of prime editors at heterochromatic sequences is contributed by their pegRNA component. In contrast, for most target sequences tested, base editing activities were similar at euchromatin and heterochromatin or, often, were even higher at the latter closed chromatin conformation. Finally, our experiments reveal that not only base editing activity as such, but also the proportions between different types of base-editing byproducts are dependent on the epigenetic status of target sequences.

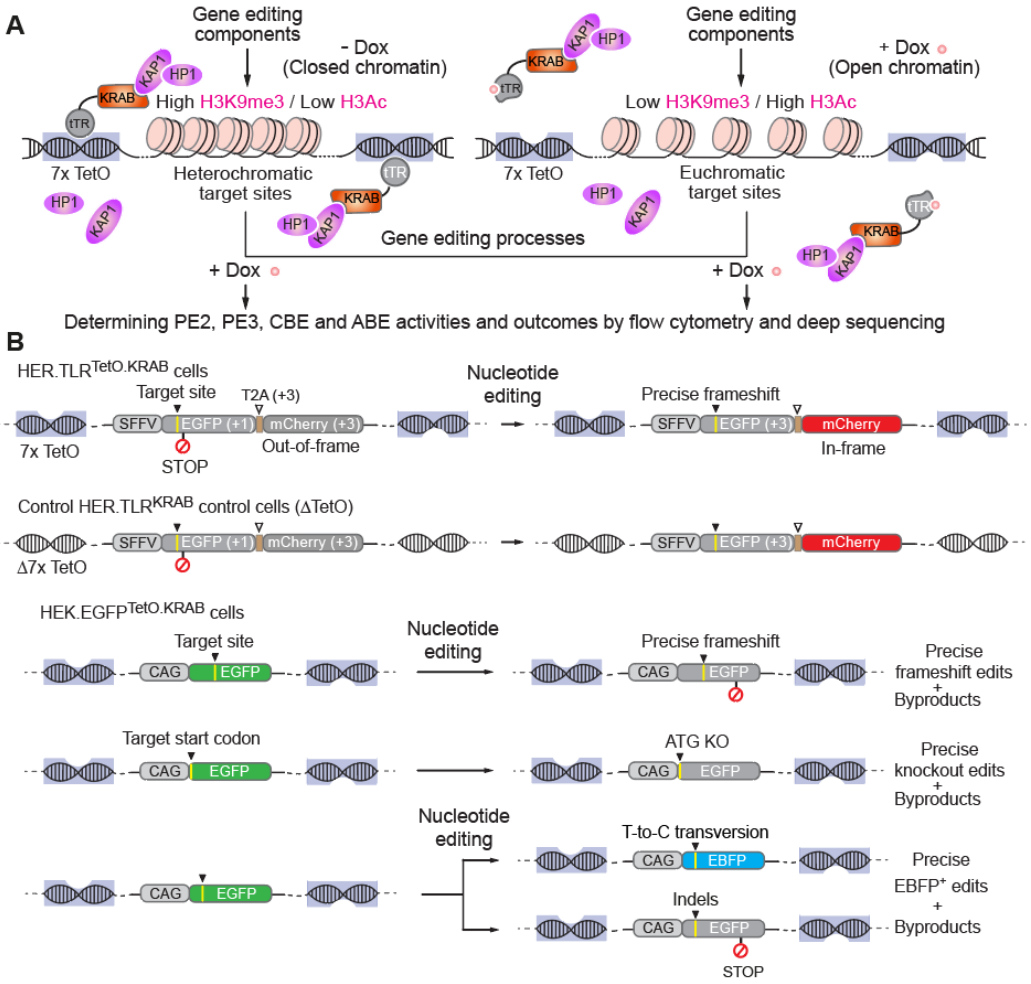

Figure 1. Experimental systems for tracing gene-editing activities and outcomes at isogenic target sequences at different chromatin conformations. (A) General experimental set-ups. Human reporter cells HER.TLR$^{TetO.KRAB}$ and HEK.EGFP$^{TetO.KRAB}$ cultured without or with doxycycline (Dox), are exposed to DSB-free gene editing tools in the form of PE2:pegRNA prime editing

complexes alone (PE2 system) or together with an auxiliary gRNA (PE3 system) or to CBE:gRNA or ABE:gRNA base editing complexes. In the absence of Dox, tTR-KRAB binds to *TetO* elements imposing a closed heterochromatic state (high H3K9me3/low H3-acetylation) at target sequences upon the recruitment of KAP1 and HP1 amongst other endogenous chromatin remodelling factors. In the presence of Dox, tTR-KRAB does not bind *TetO* permitting the same target sequences to acquire an open euchromatic state (low H3K9me3/high H3-acetylation). Once the different DNA editing processes are finished, Dox is added for determining the frequencies and types of DNA changes via flow cytometry and targeted deep sequencing analyses. **(B)** Overview of specific experimental set-ups. The tTR-KRAB-expressing HER.TLR$^{TetO.KRAB}$ cells have a *TetO*-flanked traffic light reporter (*TLR*) containing the *EGFP* reading frame interrupted by heterologous sequences and a stop codon linked to a T2A peptide "self-cleavage" motif and an out-of-frame *mCherry* reporter. Programmed DNA insertions upstream of the stop codon placing the *mCherry* in-frame are measured through mCherry-directed flow cytometry. The control tTR-KRAB-expressing HER.TLR^{KRAB} cells differ from HER.TLR$^{TetO.KRAB}$ cells in that they have a Dox-insensitive *TLR* reporter due to their lack of *cis*-acting *TetO* elements. The *TetO*-flanked *EGFP* construct in tTR-KRAB-expressing HEK.EGFP$^{TetO.KRAB}$ cells is functional with programmed frameshifts and start codon knockouts yielding a traceable EGFP-negative phenotype. DNA editing byproducts disrupting the reading frame or EGFP spectral characteristics (e.g., indels, unintended nucleotide substitutions inside and outside base editing windows, and pegRNA scaffold-derived insertions) contribute to the EGFP-negative cell fraction. In addition, in HEK.EGFP$^{TetO.KRAB}$ cells, precise T-to-C transition events at a specific codon yield a traceable blue light-emitting phenotype resulting from the conversion of the EGFP fluorophore to that of EBFP.

RESULTS

Cell- and DNA-level assays relying on defined epigenetic control over nucleotide target sequences were implemented for quantifying and characterizing genetic changes resulting from the interactions of DNA cutting-free gene editing tools with different higher-order chromatin states (**Figure 1A**). These systems, based on human embryonic kidney cells and retinoblasts (i.e., HEK.EGFP$^{TetO.KRAB}$ and HER.TLR$^{TetO.KRAB}$, respectively), allow live-cell quantification of different DNA editing outcomes (precise or otherwise) through reporter-directed flow cytometry (**Figure 1A**). The precision of the different DNA editing processes can be further analysed via genotyping assays based on deep next-generation sequencing **(Figure 1A**). In brief, in the absence of doxycycline (Dox), target sequences are embedded in heterochromatin impinged by the KRAB-mediated recruitment of KRAB-associated protein 1 (KAP-1) and heterochromatin protein-1 (HP-1) amongst other factors. This compact chromatin state is characterized by high and low deposition of specific epigenetic marks, e.g., H3K9me3 and pan H3-acetylation, respectively[29]. Conversely, in the presence of Dox, the same target sequences are placed in relaxed euchromatin characterized instead by low and high accumulation of H3K9me3 and H3-acetylation, respectively[29].

We started by transfecting HER.TLR$^{TetO.KRAB}$ and control HER.TLR^{KRAB} cells, cultured in the presence or in the absence of Dox (**Figure 1B** and **Supplementary Figure S3**), with expression plasmids expressing PE2 or PE3 components (**Figure 2A**). HER.TLR$^{TetO.KRAB}$ and HER.TLR^{KRAB} cells differ from each other in that the latter lacks *cis*-acting *TetO* elements and, as a result, target sequences retain an euchromatic character with and without Dox (**Figures 1A**). Parallel cell cultures transfected with constructs expressing control reagents (i.e., Cas9^{H840A} and non-targeting gRNA^{NT}), served as negative controls. After the action of the various complexes, all cell cultures were exposed to Dox to allow for prime editing quantification by mCherry-directed flow cytometry (**Figure 1B** and **Supplementary Figure S3**). The resulting data revealed that, in HER.TLR$^{TetO.KRAB}$ cells, prime editing activities induced by PE2 and PE3 complexes were readily detected at target sequences embedded in euchromatin whereas that was not the case at the same target sequences located in heterochromatin (**Figure 2B**, left panel). Importantly, there were no statistically significant differences in prime editing frequencies in control HER.TLR^{KRAB} cells whose target sequences are not under KRAB-dependent epigenetic control (**Figure 2B**, right panel). Similar experiments performed with another set of PE2 and PE3 reagents (**Figure 2C**) in HEK.EGFP$^{TetO.KRAB}$ cells led to results consistent with those obtained in HER.TLR$^{TetO.KRAB}$ cells (**Figure 2B**, left panel). Specifically, prime editing activities at various heterochromatic target sites were significantly lower than those attained at their euchromatic counterparts with, in fact, one of the PE2 complexes (i.e., PE2:pgRNA.31) failing to trigger prime editing above background levels at heterochromatin (**Figure 2D**). As a consequence, in HEK.EGFP$^{TetO.KRAB}$ cells, the ratios between prime editing levels corresponding to epigenetically open versus closed DNA, herein named the chromatin impact index, varied substantially, i.e., from 2- to 5.3-fold (**Figure 2E**).

To assess the relationship between prime edits and prime editing bystander events directly in living cells, we tested PE2 and PE3 complexes containing pegRNA.16 designed to change the EGFP fluorophore to that of EBFP (**Figure 1B** and **Figure 3A**). In line with the previous data (**Figure 2B**, left panel and **Figure 2D**), prime editing with these additional reagents was highest at euchromatin (**Figure**

3B, top panel; and **Figure 3C**) that, as a result, invariably led to chromatin impact indexes superior to 1 (**Figure 3D**, top panel). Notably, this enhanced prime editing activity at euchromatin was accompanied by a significant increase in gene knock-out byproducts in cells treated with the PE3 reagents (**Figure 3B**, bottom panel; and **Figure 3C**), resulting in chromatin impact indexes higher than 1 for these unintended bystander events (**Figure 3D**, bottom panel). The higher prime editing activity of PE2:pegRNA.16 complexes at euchromatin over heterochromatin was confirmed by NGS analysis (**Figure 3E**). In addition, NGS analysis identified indels at the heterochromatic and euchromatic forms of the PE2:pegRNA.16 target site as well as pegRNA scaffold-derived insertions at the latter form (**Figure 3E**).

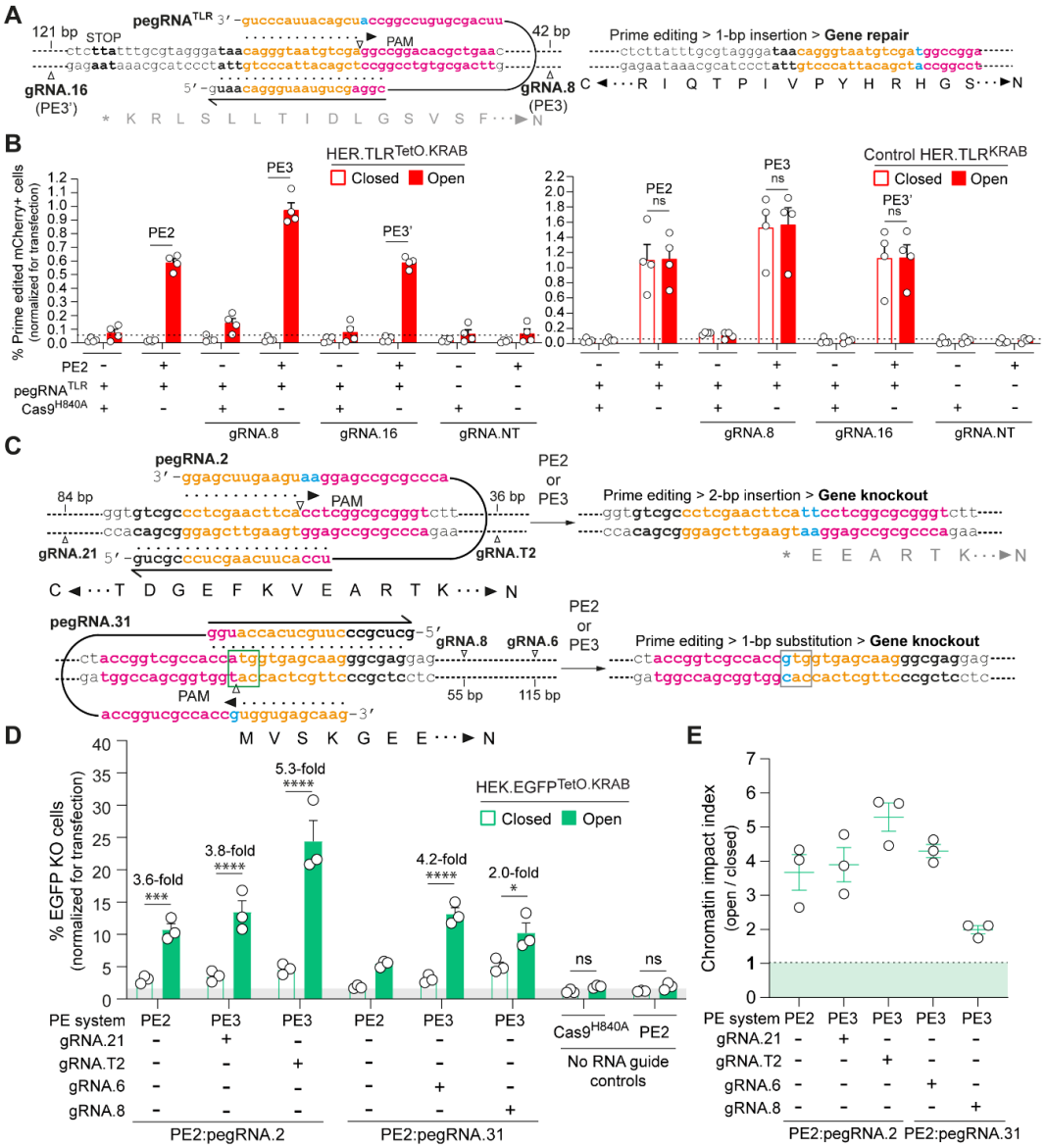

Figure 2. Prime editing at euchromatin versus heterochromatin using gene repair and gene knockout assays. (A) Gene repair set-up. Schematics of target site before and after prime editing with PE2:pegRNA^{TLR} complexes alone (PE2 system) or together with an auxiliary gRNA (PE3 system). Distances (in bp) between nicks defined by pegRNA^{TLR} and each auxiliary gRNA are specified. pegRNA^{TLR} is built to correct the *mCherry* reading frame by inserting a 1-bp (cyan nucleotides). **(B)** Quantification of prime editing in human embryonic retinoblasts. HER.TLR$^{TetO.KRAB}$ and control HER.TLR^{KRAB} cells (left and right panel, respectively), treated and not treated with Dox, received the indicated prime-editing and control reagents. mCherry-directed flow cytometry after sub-culturing and Dox addition establishes prime editing frequencies. Bars and error bars correspond to mean ± s.e.m., respectively (n=4 biological replicates); $P > 0.05$ considered non-significant (ns). (**C**) Gene knockout set-ups. Schematics of pegRNA.2 and pegRNA.31, and their respective target sites, before and after prime editing. Distances (in bp) between nicks defined by pegRNAs and pairing gRNAs for PE3-based DNA editing are shown. pegRNA.2 and pegRNA.32 are designed for target gene knockout through the installation of a 2-bp insertion and a 1-bp substitution that disrupts the reading frame and start codon, respectively (cyan nucleotides). **(D)** Quantification of prime editing in human embryonic kidney cells. HEK.EGFP$^{TetO.KRAB}$ cells, cultured with or without Dox, received the indicated prime-editing and control reagents. Flow cytometry upon sub-culturing and Dox addition established EGFP knockout frequencies. Bars and error bars represent mean ± s.e.m., respectively (n=3 biological

replicates). Significances derived from two-way ANOVA followed by Šídák's test for multiple comparisons; *0.01 < *P* < 0.05; ***0.0001< *P* < 0.001; ****P < 0.0001; P > 0.05 was considered non-significant (ns). **(E)** Relative prime editing activities at open versus closed chromatin. Chromatin impact indexes for the indicated PE2 and PE3 reagents corresponding to the ratios between the mean EGFP knockout frequencies measured in the presence and absence of Dox. Scatter plot displays mean ± s.e.m. (n=3 biological replicates).

Delivery of PE3 RNA reagents together with $Cas9^{H480A}$, instead of PE2, also yielded a significant increase in byproduct accumulation at euchromatin (**Figure 3B**, bottom panel). This data supports the conclusion that most PE3-induced mutagenic events arose from offset nicking at both DNA strands and that these mutagenic events were most prevalent at euchromatin. Interestingly, the 6.3-fold higher prime editing activities at heterochromatin using PE2, pegRNA.16 and gRNA.2, instead of PE2 and pegRNA.16 (**Figure 3B**, top graph), was not accompanied by a significant increase in byproduct build-up (**Figure 3B**, bottom graph). This data suggests that, at certain heterochromatic sequences, judicious selection of auxiliary gRNAs can lead to efficient PE3-mediated editing without a concomitant build-up of DSB-derived indels. Taken together, these data indicate that prime editing is hindered at KRAB-impinged heterochromatin in a target site- and PE system-independent manner.

Next, we sought to probe the capacity of pegRNAs to engage different chromatin states by coupling them to Cas9. To this end, $HER.TLR^{TetO.KRAB}$ and $HER.TLR^{KRAB}$ cells, cultured with or without Dox, were exposed to Cas9 together with $gRNA^{TLR}$ or $pegRNA^{TLR}$ whose spacer and scaffold sequences are the same. At both chromatin states, reading frame repair resulting from Cas9-induced indels was lowest in cells receiving $pegRNA^{TLR}$ (**Figure 4A**, left panel). Moreover, when compared to canonical $Cas9{:}gRNA^{TLR}$ complexes, $Cas9{:}pegRNA^{TLR}$ complexes were the most hindered by heterochromatin (**Figure 4A**, left panel), as highlighted by their 5.4-fold higher chromatin impact index (**Figure 4A**, right panel). In control $HER.TLR^{KRAB}$ cells, significant differences in DNA editing events between cultures treated and untreated with Dox were, once again, not detected regardless of the tools used (**Figure 4B**). Similar experiments performed in $HEK.EGFP^{TetO.KRAB}$ cells with another set of gRNAs and pegRNAs sharing the same spacers, yielded outcomes consistent with those obtained in $HER.TLR^{TetO.KRAB}$ cells (**Figure 4C**). Firstly, at both chromatin states, gene knockouts resulting from Cas9-induced indels were lowest in cells receiving pegRNAs instead of gRNAs (**Figure 4C** and **Figure 4D**). And, secondly, when compared to canonical Cas9:gRNA complexes, Cas9:pegRNA complexes were the most impeded by heterochromatin (**Figure 4C**), as underscored by their 2-fold higher chromatin impact indexes (**Figure 4E**). Taken together, these data shows that pegRNAs can contribute to the underperformance of prime editing complexes at KRAB-regulated heterochromatin.

Tethering KRAB domains to chromosomal sequences through DNA-binding motifs of native and engineered proteins (e.g., zinc-finger-KRAB and tTR-KRAB proteins, respectively) can locally nucleate *bona fide* heterochromatin[29,33-35]. However, the resulting heterochromatin is not maintained if pioneering KRAB-containing proteins are solely recruited. Thus, clearly, additional epigenetic factors are necessary for depositing specific combinations of DNA methylation and histone modifications that, together, underpin stable and heritable heterochromatic states. Importantly, a single fusion protein named CRISPRoff consisting of a catalytically "dead" Cas9 scaffold linked to KRAB and to two DNA methyltransferases (i.e., DNMT3A and DNMT3L), has recently been shown to assemble stable heterochromatin through RNA-programmable binding to endogenous gene control regions[36]. Hence, to further study the role of chromatin controlled by specific epigenetic factors on prime editing, we next applied the CRISPRoff system to epigenetically remodel *CD81* alleles. To this end, after exposing HEK293T cells to CRISPRoff and gRNAs targeting *CD81* regulatory sequences (**Supplementary Figure S4**), cells acquiring a $CD81^-$ phenotype were sorted from their $CD81^+$ counterparts via FACS (**Figure 5A**). The sorted $CD81^-$ and $CD81^+$ cell populations kept their respective phenotypes upon long-term culturing (**Figure 5B**). Importantly, as demonstrated by ChIP-qPCR analyses, $CD81^-$ and $CD81^+$ cells contained *CD81* alleles with epigenetic marks characteristic of heterochromatin and euchromatin, respectively. Specifically, *CD81* sequences in $CD81^-$ cells were enriched in histone 3 lysine 9 trimethylation (H3K9me3) and depleted in histone 3 acetylation (H3Ac) (**Figure 5C**). Conversely, *CD81* sequences in $CD81^+$ cells were depleted in H3K9me3 and enriched in H3Ac (**Figure 5C**). The $CD81^-$ and $CD81^+$ cell populations were transfected with constructs expressing prime editing complexes (n=10), designed to install 1-bp substitutions at epigenetically silenced and active *CD81* alleles, respectively (**Figure 5D**). Western blot analysis with a Cas9-specific antibody confirmed similar prime editor expression levels (**Figure 5E**), and the absence of otherwise interfering CRISPRoff complexes in

the CD81⁺ and CD81⁻ cells (**Figure 5E**, Mock lanes). Deep sequencing analysis revealed that amongst the ten prime editing complexes assembled, seven yielded higher prime editing activities in CD81⁺ than in CD81⁻ cells (up to 2.8-fold); with statistical significance being reached in cells exposed to five of these complexes (**Figure 5F**). In contrast, the higher prime editing activities measured in CD81⁻ than in CD81⁺ cells resulting from the three additional prime editing complexes did not reach statistical significance (**Figure 5F**). Taken these data together, we conclude that prime editing is mostly unfavoured at heritable heterochromatin controlled by the combined recruitment of KRAB and DNA methyltransferases DNMT3A and DNMT3L.

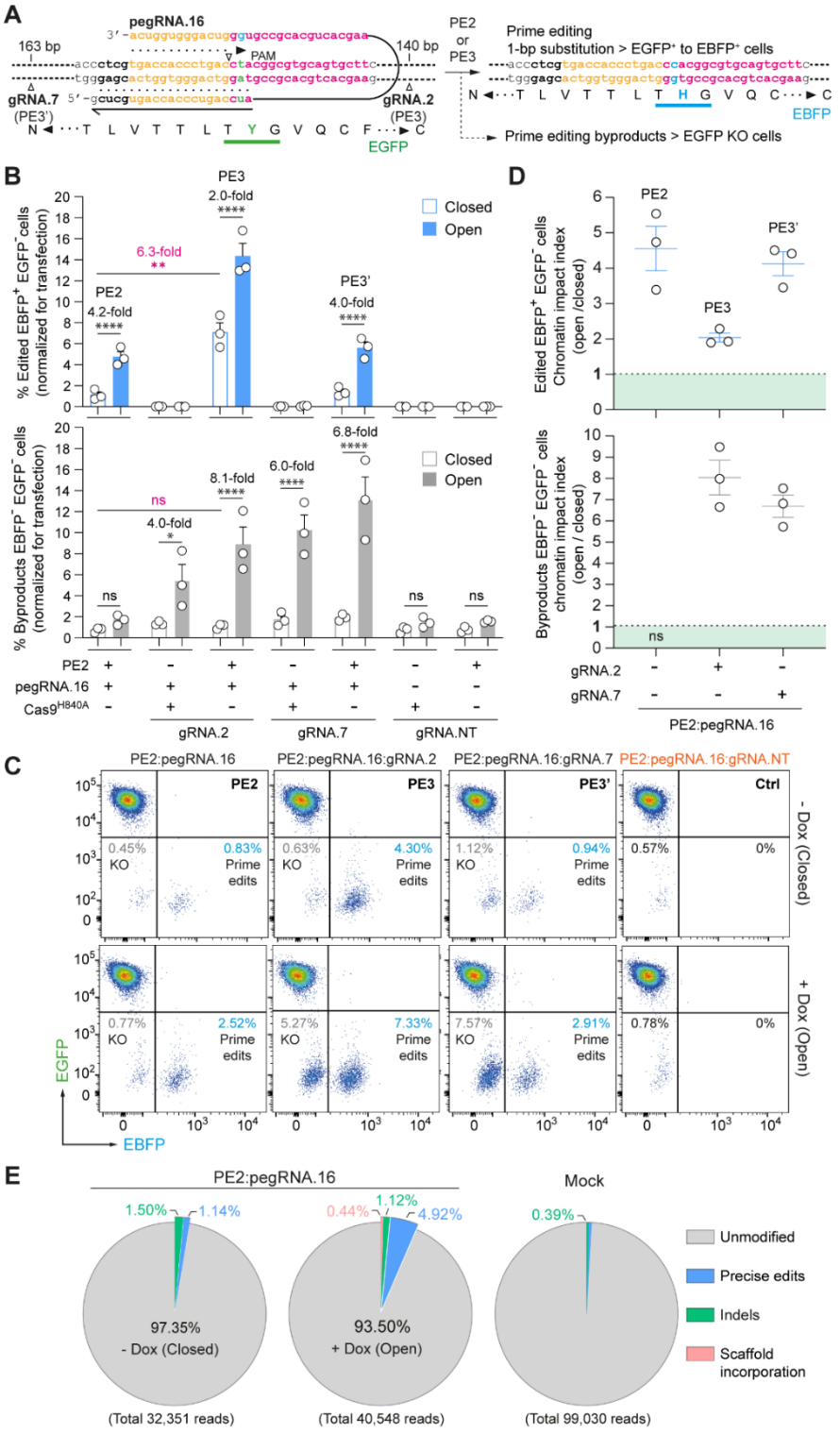

Figure 3. Prime editing outcomes at euchromatin versus heterochromatin combining live-cell gain and loss of function assays. (A) Prime editing set-up. Schematics of pegRNA.16 and cognate target sequence before and after prime editing with PE2:pegRNA.16 complexes alone (PE2 system) or together with an auxiliary gRNA (PE3 system). Distances (in bp) between nicks defined by pegRNA.16 and each auxiliary gRNA are specified. pegRNA.16 is designed to change the fluorophore of EGFP to that of EBFP (underlined residues). **(B)** Flow cytometric quantification of prime editing outcomes. HEK.EGFP$^{TetO.KRAB}$ cells, treated or not treated with Dox, were exposed to the indicated prime-editing or control components. Flow cytometry after sub-culturing and Dox supplementation quantified prime editing (i.e., EBFP-positive cells) and gene knockout by-product events (i.e., EBFP/EGFP doubly negative cells). Bars and error bars represent mean ± s.e.m., respectively (n=3 biological replicates). Significance between - and + doxycycline datasets derived from two-way ANOVA followed by Šídák's test for multiple comparisons; *0.01 < *P* < 0.05; ****P < 0.0001; P > 0.05 considered non-significant (ns). Significance between the indicated - doxycycline datasets was determined with two-tailed Student's t test; **0.001 < *P* < 0.01; P > 0.05 considered non-significant (ns). **(C)** Representative dot plots corresponding to the experimental results plotted in panel B. **(D)** Relative prime editing outcomes at open versus closed chromatin. Chromatin impact indexes corresponding to prime editing and indel-derived gene knockout events at open and closed chromatin (top and bottom panel, respectively) induced by the indicated components. Scatter plots display mean ± s.e.m. (n=3 biological replicates). (**E**) Deep sequencing quantification of prime editing outcomes. Pie chart parsing the frequencies of prime editing events in HEK.EGFP$^{TetO.KRAB}$ cells treated and untreated with Dox and exposed to PE2:pegRNA.16 complexes. Mock-transfected cells served as negative control.

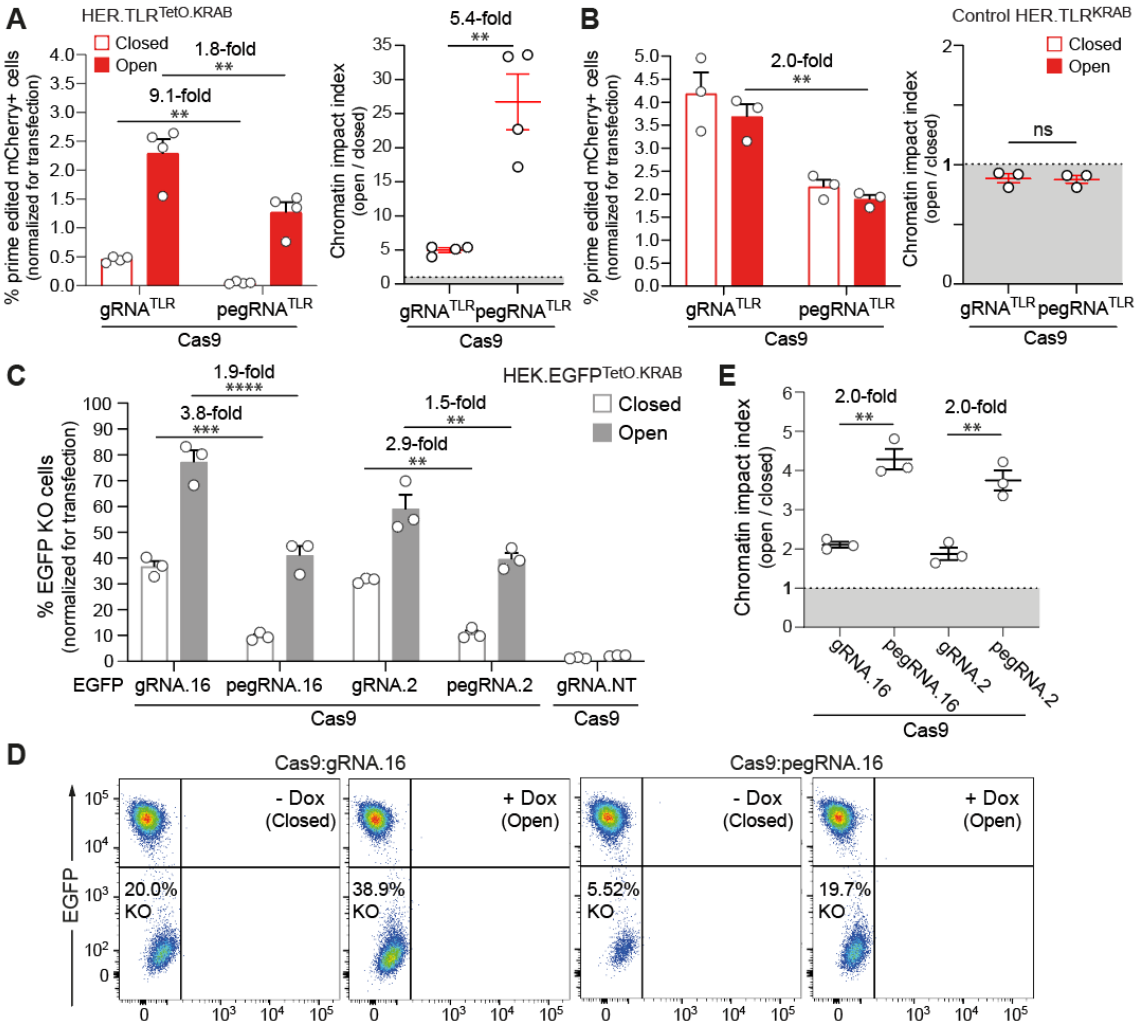

Figure 4. Probing the performances of gRNAs versus pegRNAs at euchromatin and heterochromatin. (**A**) Gain-of-function assessments in HER.TLR$^{TetO.KRAB}$ cells. Cells treated and untreated with Dox received either canonical Cas9:gRNA^{TLR} or Cas9:pegRNA^{TLR} complexes. After sub-culturing and Dox supplementation, flow cytometry quantified Cas9-mediated correction of the *mCherry* reading frame. Gene repair frequencies and corresponding chromatin impact indexes are plotted. (**B**) Gain-of-function assessments in control HER.TLR^{KRAB} cells. The same procedures and reagents applied to HER.TLR$^{TetO.KRAB}$ were also used in *TetO*-negative HER.TLR^{KRAB} control cells. Gene repair frequencies and corresponding chromatin impact indexes are plotted. (**C**) Loss-of-function assessments in HEK.EGFP$^{TetO.KRAB}$ cells. Cells cultured with and without Dox, were exposed to the indicated reagents. Flow cytometry after sub-culturing and Dox addition established Cas9-induced EGFP knockout frequencies. (**D**) Representative dot plots corresponding to experimental results shown in panel C. (**E**) Relative gene knockout levels at open versus closed chromatin. Chromatin impact indexes for the indicated reagents were assessed by calculating the ratios between the mean EGFP knockout levels measured in the presence and absence of Dox. Results are depicted as mean ± s.e.m. of 3 or 4 independent biological replicates. Significances amongst gene repair and gene knockout datasets were calculated via two-way ANOVA followed by Šídák's test for multiple comparisons. Significances between chromatin impact index datasets were

determined with unpaired two-tailed Student's t test. **0.001 < P < 0.01; ***0.0001< *P* <0.001; ****$P < 0.0001$; $P > 0.05$ considered non-significant (ns).

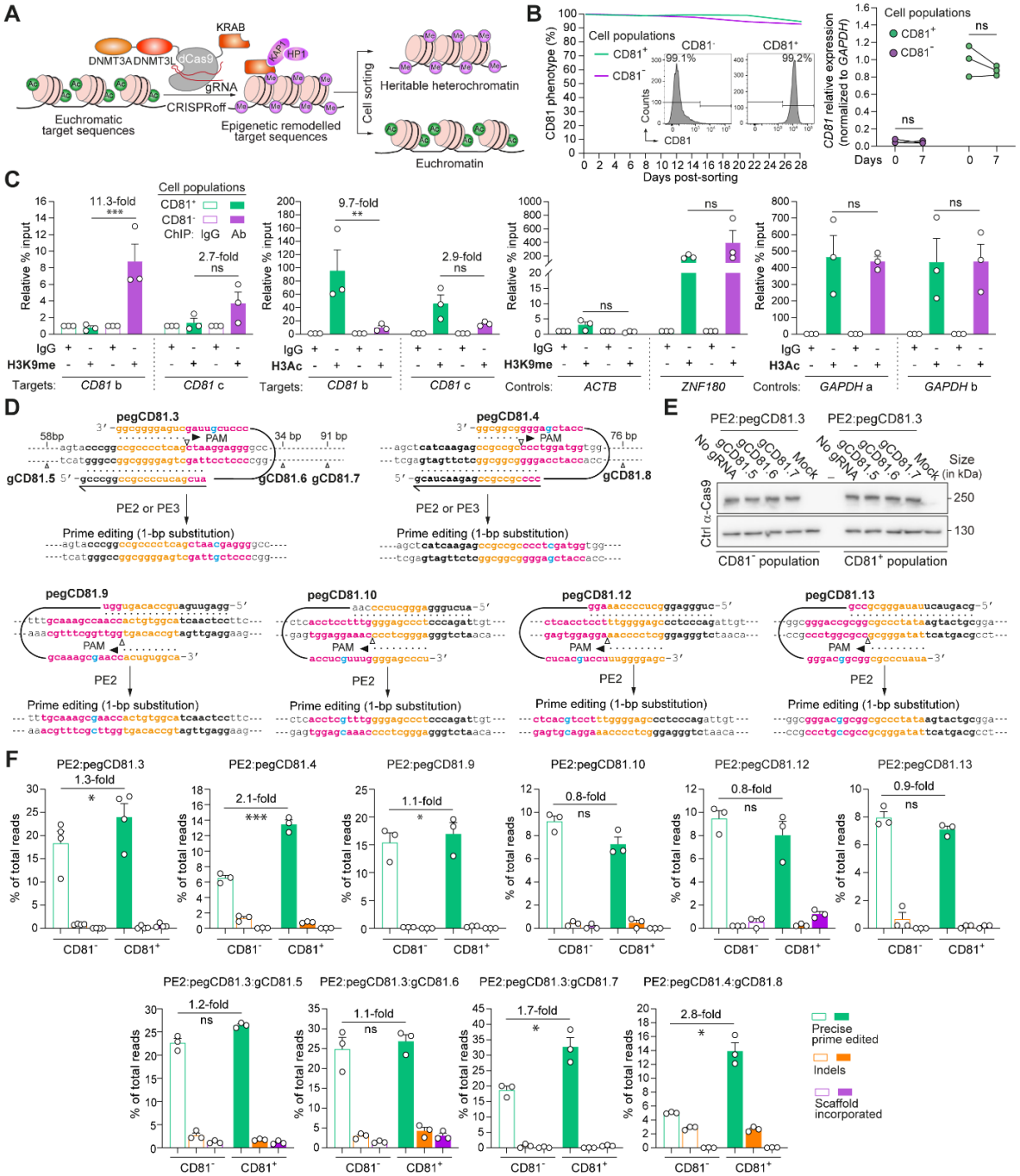

Figure 5. Prime editing at open and heritable closed chromatin. (**A**) Illustration of experimental set-up. HEK293T cells with *CD81* in epigenetically open and closed states were generated through CRISPRoff transfection and CD81-based cell sorting (CD81$^+$ and CD81$^-$ populations, respectively). (**B**) Validation of stable CD81 phenotypes. CD81$^+$ and CD81$^-$ phenotypes are maintained upon sub-culturing as assessed through flow cytometry and RT-qPCR analyses (left and right panel, respectively). Inset, representative flow cytometry histogram. Significances were calculated via two-way ANOVA followed by Šídák's test for multiple comparisons. $P > 0.05$ considered non-significant (ns). (**C**) Validation of stable *CD81* epigenetic states. ChIP-qPCR analyses of two *CD81* regions in CD81$^+$ and CD81$^-$ cells presenting preferential enrichment of the heterochromatin mark H3K9me3 in the former; and the euchromatin mark pan-H3 acetylation (H3Ac) in the latter. ChIP-qPCR analyses controls involved assessing H3K9me3 and H3Ac marker deposition at loci with known open chromatin (i.e., *ACTB* and *GAPDH*) and closed chromatin (i.e., *ZNF180*) conformations. ChIP-qPCR data, controlled for background (IgG) and normalized for input chromatin, are plotted as mean ± s.e.m. of percentage of input values (n=3 technical replicates). Significances were calculated via two-way ANOVA followed by Tukey's test for multiple comparisons. **0.001 < *P* < 0.01; ***0.0001< *P* <0.001; $P > 0.05$ considered non-significant (ns). (**D**) Prime editing set-ups at *CD81*. Schematics of pegRNA.CD81.1 and pegRNA.CD81.2 and their respective target sites prior to and after prime editing. Distances (in bp) between nicks defined by pegRNAs and each pairing gRNA for PE3-based DNA editing are also depicted. *CD81*-targeting pegRNAs are designed for installing G-to-C substitutions at two separate

places within the gene (cyan nucleotides). (**E**) Controlling chromatin-remodelling and prime-editing complex levels. Western blot analysis confirming the absence of CRISPRoff proteins in long-term cultures of CD81$^-$ and CD81$^+$ cells (Mock) and establishing similar amounts of prime editors in these cultures at 48 h post-transfection. (**F**) Quantification of prime editing at alleles with heritable open and closed chromatin. Targeted deep sequencing analysis of CD81$^-$ and CD81$^+$ cells at 7 days post-transfection of constructs expressing the indicated PE2 and PE3 complexes. Mock-transfected cells served as negative controls. Bars and error bars represent mean ± s.e.m., respectively, of 3 independent biological replicates. Significances between indicated datasets were determined with paired two-tailed Student's t test. *0.01 < *P* < 0.05; ***0.0001< *P* <0.001; *P* > 0.05 considered non-significant (ns).

To start investigating the performance of base editors at euchromatin versus heterochromatin, HEK.EGFP$^{TetO.KRAB}$ cells cultured with or without Dox, were transfected with constructs expressing CBE or ABE complexes designed for *EGFP* knockout through site-directed mutagenesis (**Supplementary Figure S5**). Strikingly, flow cytometry analysis readily disclosed that, when compared to prime editing complexes, base editing complexes are typically the least affected at heterochromatin (**Figure 6A**). Indeed, amongst the eight base editors initially assembled, six presented either similar efficiencies at euchromatin and heterochromatin or even higher efficiencies at the latter compact DNA state (**Figure 6A**) yielding, as a result, chromatin impact indexes around or under 1, respectively (**Figure 6B**). The fluorophore exchange capacity of ABE:gRNA.32 was further explored to confirm its similar performance at euchromatin and KRAB-regulated heterochromatin via flow cytometric quantification of cells acquiring EBFP-specific fluorescence (**Figure 6C** and **Figure 6D**).

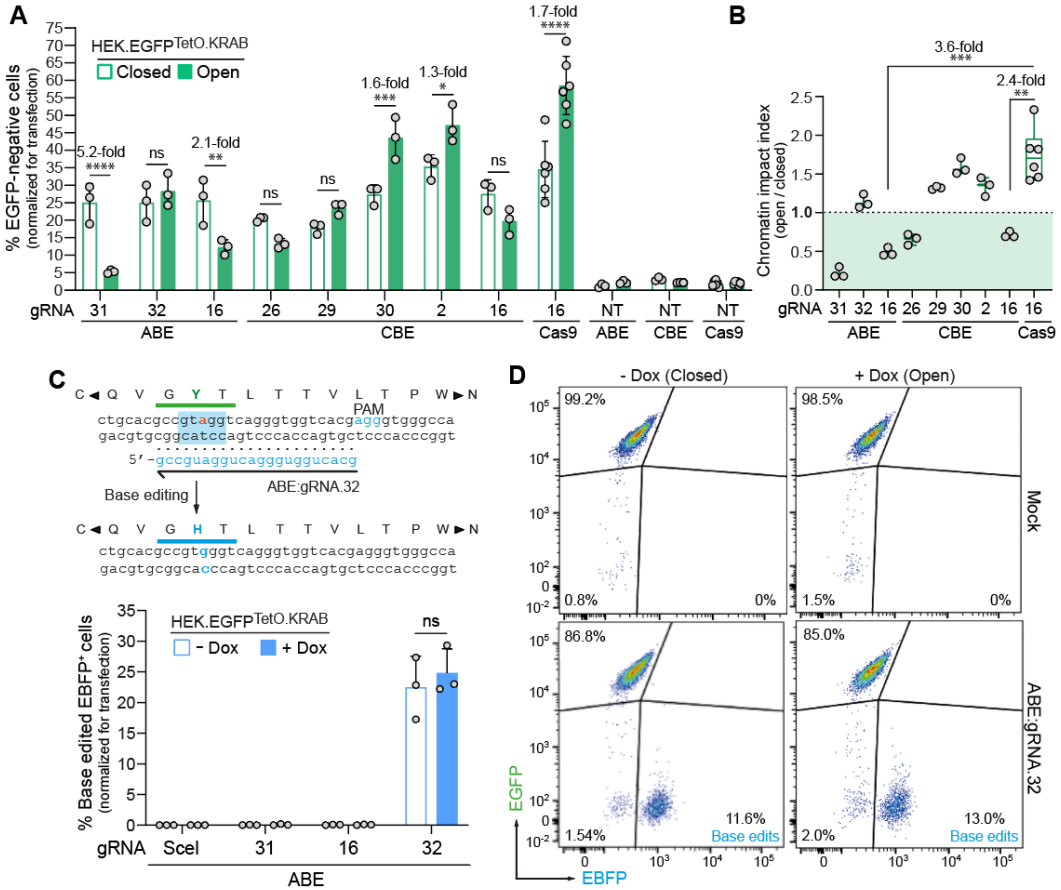

Figure 6. Investigating base editing at euchromatin versus heterochromatin with combined loss and gain of function live-cell assays. (**A**) Gene knockout set-ups. HEK.EGFP$^{TetO.KRAB}$ cells, cultured with or without Dox, were treated with the indicated base-editing and control reagents. Flow cytometry upon sub-culturing and Dox addition established EGFP knockout frequencies. Bars and error bars denote mean ± s.d. of independent biological replicates, respectively. Significances were calculated via two-way ANOVA followed by Šídák's test for multiple comparisons; *0.01 < *P* < 0.05; **0.001 < *P* < 0.01; ***0.0001< *P* < 0.001; ****P < 0.0001; P > 0.05 considered non-significant (ns). **(B)** Relative base editing activities at open versus closed chromatin. Chromatin impact indexes for the indicated base-editing and control reagents correspond to the ratios between the mean EGFP knockout levels measured in the presence and absence of Dox. Scatter plot displays mean ± s.d. Significances were calculated via Student's *t* test; **0.001 < *P* < 0.01; ***0.0001< *P* < 0.001 **(C)** Gene conversion set-ups. Schematics of gRNA.32 and cognate target sequence before and after prime editing with ABE:gRNA.32 complexes. Target and product nucleotides withing the editing window are marked in red and cyan, respectively. gRNA.32 (spacer shown) is designed to change the fluorophore of EGFP to that of EBFP (underlined residues). HEK.EGFP$^{TetO.KRAB}$ cells, treated or not treated with Dox, were exposed to ABE:gRNA.32. EBFP-directed flow cytometry after sub-culturing and Dox addition established base editing frequencies. Significance was assessed by using

two-tailed Student's t test; *P* > 0.05 was considered non-significant (ns). **(D)** Representative dot plots corresponding to experimental data plotted in panel C.

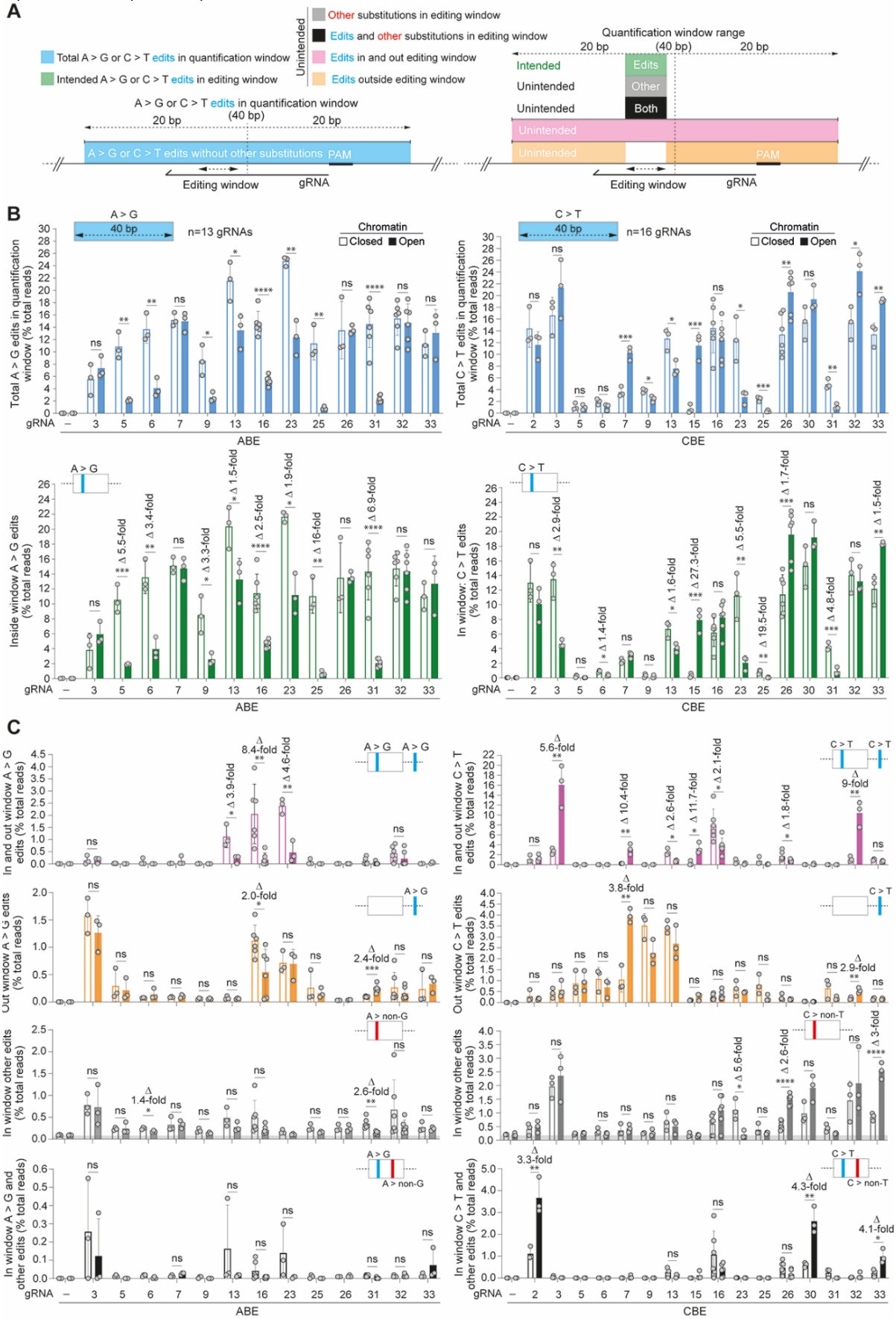

Figure 7. Base editing at open and KRAB-controlled closed chromatin. (**A**) Diagram of the distribution of intended and unintended base-editing products. Base edits (i.e., A > G or C > T) within quantification and editing windows are labelled in cyan and green, respectively. A > G or C > T base edits present simultaneously inside and outside editing windows are marked in magenta and A > G or C > T base edits present exclusively outside editing windows are labelled in orange. Unintended substitutions (i.e., A > non-G and C > non-T) within editing windows (other) are marked in grey. Composite edits consisting of intended and unintended substitutions inside editing windows are labelled in black. (**B**) Quantification of base edits at open and KRAB-controlled closed chromatin. HEK.EGFP$^{TetO.KRAB}$ cells incubated with or without Dox were exposed to the indicated ABE:gRNA and CBE:gRNA complexes designed for installing A > G and C > T substitutions, respectively. Total base edits within the quantification window and intended base edits within each editing window are plotted (top and bottom graphs, respectively). (**C**) Quantification of base-editing byproducts at open and KRAB-controlled closed chromatin. Base-editing byproducts corresponding to base edits inside and outside editing windows or only outside these windows are plotted as magenta and orange bar graphs, respectively. Base-editing byproducts corresponding to unintended substitutions and composite edits consisting of intended and unintended substitutions are plotted as grey and black bar graphs. Base editing events were measured through deep sequencing analyses (50,000 paired-end reads). Significances were determined via two-tailed Student's *t* tests with bars and error bars corresponding to mean ± s.d., respectively (n=3 biological replicates). $P > 0.05$ considered non-significant (ns).

Bystander effects created by ABEs and CBEs include conversion of base pairs outside their predicted editing windows and conversion of target-to-unintended base pairs inside and/or outside those editing windows (i.e., A·T and C·G changing to base pairs other than G·C and T·A, respectively) that, as a consequence, reduce their precision and product purity, respectively (**Figure 7A**). The frequencies and proportions between intended and unintended bystander events and between the different types of the latter products ultimately determines the performance of specific base editing reagents. Notably, whether the epigenetic context of nucleotide sequences affects these key base-editing parameters remains an open question. To address this question, an expanded panel of ABE and CBE complexes, was applied to isogenic target sequences placed in euchromatin versus KRAB-regulated heterochromatin using the HEK.EGFP$^{TetO.KRAB}$ cell system (n=29) (**Figure 7B** and **Supplementary Figure S6**); or embedded in euchromatin versus heritable heterochromatin controlled by the combined actions of KRAB, DNMT3A and DNMT3L using the CD81^{+}/CD81^{-} HEK293T cell system (n=9) (**Supplementary Figures S7** and **S8**). Deep sequencing analyses of A > G and C > T edits within a 40-bp quantification window and within the canonical ABE and CBE base editing windows (**Figure 7A**, cyan and green bins, respectively) confirmed that, diversely from prime editing, base editing activities at heterochromatin are frequently as high as or higher than those registered at euchromatin (**Figure 7B** and **Supplementary Figure S8A**). Indeed, the installation of the intended ABE- and CBE-derived edits was mostly either unhindered (i.e., 5/13 and 6/16, respectively) or in fact fostered (i.e., 8/13 and 5/16, respectively) at heterochromatin, resulting in a majority of base editing complexes presenting a chromatin impact index at or below 1, respectively (**Figure 8**). Remarkably, amongst the ABE and CBE complexes tested, only ABE:gRNA.81.11 (1/17) and 6 CBE:gRNA complexes (6/21), respectively, led to higher base editing at euchromatin than heterochromatin (**Figure 7B** and **Supplementary Figure S8A**).

Further deep sequencing analyses directed at investigating cause-effect relationships between alternate chromatin states and the modulation of base-editing byproducts parsed in 4 different categories (**Figure 7A**, magenta, orange, grey and black bins), showed that the chromatin environment can indeed significantly influence the precision and purity attained by base editors in a gRNA-dependent manner (**Figure 7C** and **Supplementary Figure S8B**) that results in varying proportions between base edits and different types of unintended byproducts (**Supplementary Figure S9**). Interestingly, in these cases, it was observed that diversely from ABE complexes, whose base edits inside and outside editing windows were both mostly higher in heterochromatin, CBE complexes often did not lead to a direct correlation between the frequencies of these substitutions at the two alternate chromatin states. In addition, CBE complexes presented a higher tendency for "spilling over" base editing outside their canonical windows at euchromatin when compared to their ABE counterparts (**Figure 7C**, magenta and orange bars; and **Figure 9**). Finally, consistently with earlier experiments[23], amongst the ABE and CBE complexes tested, the latter were more prone to yielding higher target-to-unintended substitutions than the former (**Figure 7C** and **Supplementary Figure S8B**, grey and black bars). Substitutions reducing CBE product purity have been linked in *Saccharomyces cerevisiae* to the action of specialized DNA polymerases that underpin mutagenic translesion synthesis (TLS)[37]. Our data further discloses that base editing product purity, controlled by TLS or other processes, can vary at alternate chromatin states in a gRNA-dependent manner.

In conclusion, in this study, we demonstrate that the chromatin environment has a significant bearing not only on the activity but also on the precision and product purity attained by DSB-free genome

engineering technologies based on prime editors and base editors. Notably, in striking contrast with programmable nucleases and prime editors, heterochromatin states can in fact favour the activities of base editing complexes.

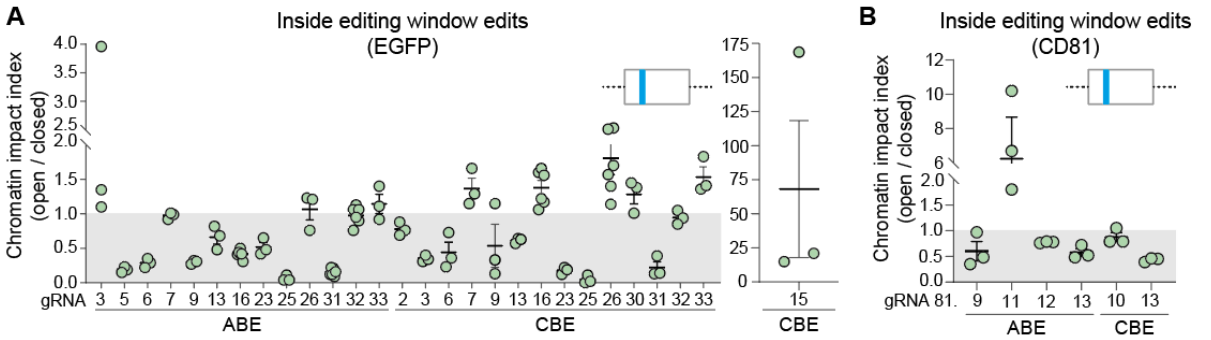

Figure 8. Relative base editing activities at open versus closed chromatin. Chromatin impact indexes for the indicated reagents corresponding to the ratios between base-editing frequencies as determined by deep sequencing at (**A**) *EGFP* and (**B**) *CD81* target sites in open and closed chromatin. Base editing frequencies were determined through amplicon deep sequencing (50,000 paired-end reads). Scatter plot displays mean ± s.d. values.

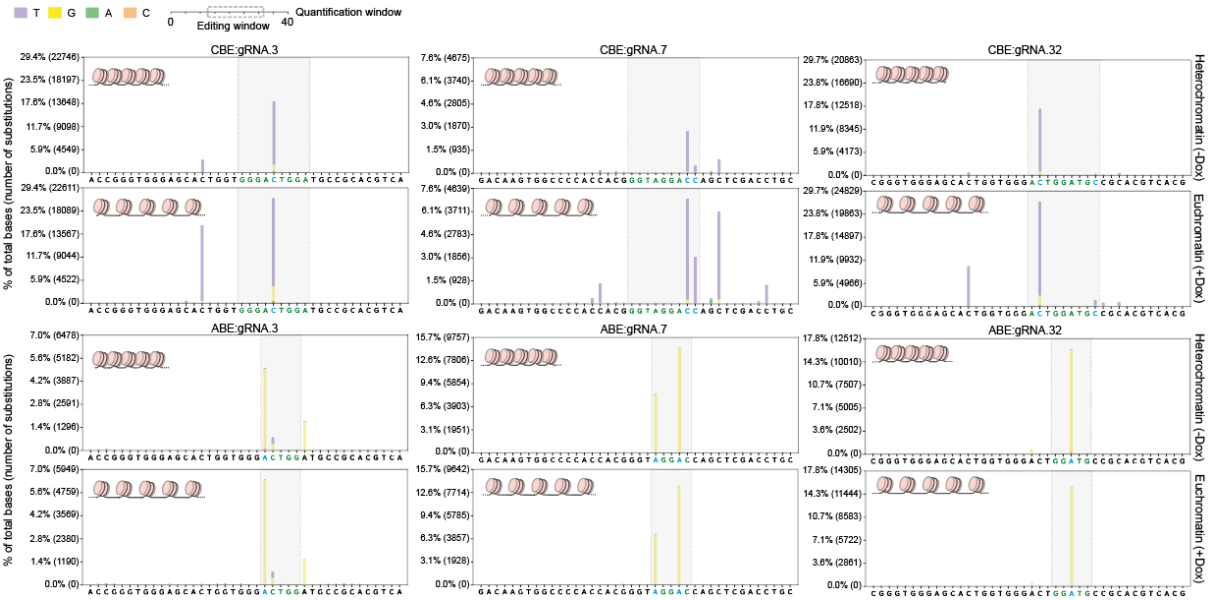

Figure 9. Characterization of base editing events. Representative histograms depicting the type, range and frequency of base editing outcomes generated by the indicated CBE and ABE complexes at open versus closed chromatin in HEK.EGFP$^{TetO.KRAB}$ cells. Green and cyan letters mark the editing window and target nucleotide sequences, respectively, for each of the base editing complexes.

DISCUSSION

The activity of genome-editing reagents is generally dependent on a combination of genetic and epigenetic variables, i.e., nucleotide sequences per se and their epigenetically-regulated chromatin environment, respectively. In this work, to strictly dissect these variables and, as a result, directly investigate the influence of higher-order chromatin conformations not only on the activity but also on the precision of prime editors and base editors, we implemented complementary cellular systems in which isogenic euchromatic and heterochromatic target sites are installed by the recruitment of well-defined epigenetic remodelling factors.

Previous studies from our laboratory and those of others have established that programmable nucleases, including those derived from CRISPR systems, are primarily active at euchromatin than heterochromatin with differential PAM and protospacer accessibility at these distinct higher-order chromatin states constituting a likely determinant factor[29-32]. Similarly to programmable nucleases, recent studies indicate that prime editors are also frequently more active at euchromatic sequences[38,39]. The findings reported here are consistent with these recent studies and further point to the extended 3' ends of pegRNAs (i.e.,

PBS and RT template sequences) as possible culprits for the underperformance of prime editors at heterochromatic sites and for their typically higher chromatin impact indexes than Cas9 nucleases. Of notice, the protection from exonucleolytic degradation of pegRNAs with structured RNA pseudoknots at their 3' ends suggests that extended pegRNA sequences protrude from prime editing complexes[40]. One can postulate that such protruding RNA sequences are more likely to become "trapped" at heterochromatic sites due to local interactions with positively charged deacetylated histone tails and, conversely, become more freely available for DNA flap hybridization and RT-driven cDNA synthesis in euchromatin owing to higher levels of negatively charged acetylated histone tails (**Supplementary Figure S10**). In addition, one can also postulate that DNA flap intermediates emerging during prime editing (**Supplementary Figure S2**), equally associate with deacetylated positively charged histones characteristic of heterochromatic states and, in doing so, contribute to dampened DNA editing. Finally, experiments using PE3 RNA reagents (i.e., pegRNA/gRNA pairs) and the Cas9^{H840A} nickase instead of the whole prime editor protein, confirmed that most mutations caused by PE3 components arise from offset nicking at both DNA chains and further disclosed that these byproducts can build-up at euchromatin.

Experiments correlating CBE BE4[21] and ABE7.10[23] efficiencies with the DNase I hypersensitive site profiling of cognate gRNA target sequences in HEK293T cells suggest that CBE activities are, on average, higher at open than at closed chromatin (1.9-fold); whilst ABE activities are barely affected by chromatin accessibility (1.1-fold). Intriguingly, when compared with their parental proteins, ABE8e-V106W[41] and ABEmax[42] base editors fused to chromatin remodelling and transcription activating domains (i.e., HMGN1 and SOX2 fusions, respectively) yielded lower, similar or higher DNA editing frequencies depending on the loci and nucleotide positions[43,44]. Variable DNA editing by CBE and ABE fusion constructs were also shown to be dependent on the type and fusion location of the effector domains selected on the basis of their involvement in chromatin relaxation[43,44]. Of notice, correlations between histone deacetylase inhibitor (HDACi) treatments and enhanced base editing at certain loci have been interpreted as the result of HDACi-dependent base editor and gRNA expression upregulation and/or increased target sequence accessibility[45,46]. However, in addition to increasing collateral off-target DNA editing[45,46], HDACi treatments have pleiotropic effects that may alter the DNA editing processes themselves via their known modulation of cellular DNA repair pathways, including BER and MMR[47]. This consideration is strengthened by the observation that HDACi treatments while increasing the activity of prime editing complexes designed for installing insertions or deletions, seem to decrease the activity of similar complexes assembled instead for the incorporation of point mutations[46]. Finally, base editors and Cas9 nucleases coupled to the same gRNA can present highly disparate activities[48,49] suggesting that additional mechanisms other than PAM and protospacer accessibility per se, contribute to modulating the efficiency of individual base editing complexes.

Independent cell- and DNA-level assays disclosed that, in striking contrast to prime editors, the activity of base editors are often either unhindered or even fostered when nucleotide sequences transition from euchromatic to heterochromatic states. In particular, heterochromatin installed by the recruitment of the KAP-1 and HP-1 scaffolding KRAB domain alone or together with the DNA methyltransferases DNMT3A and DNMT3L. This finding overtly contrasts with the aforementioned, mostly inhibitory, function of heterochromatin on the activities of CRISPR nucleases and prime editors[29-32, 38,39 and this study].

Base excision repair (BER) is a multi-set process initiated by DNA glycosylases that, through the removal of specific aberrant bases, creates abasic sites that serve as substrates for the apurinic/apyrimidinic endonuclease 1 (APE1). The resulting SSB or gap is ultimately filled-in and sealed by DNA polymerase β and DNA ligase III/XRCC1, respectively. Dissecting the molecular processes underpinning the herein reported surprising finding that base editing can be fostered at heterochromatin will require further research. In this context, it is enticing to postulate a role for heterochromatin in obstructing BER pathways that eliminate CBE and ABE deaminated nucleotides in the form of deoxyuridine and deoxyinosine/hypoxanthine, respectively. Indeed, optimized architectures of CBEs incorporate fusions to an uracil-DNA glycosylase (UDG) inhibitor (UGI) to counteract BER activity and hence improve DNA editing efficiency (**Supplementary Figure S10**). Interestingly, there are also indications that ABE and UGI fusion products can equally foster DNA editing at certain loci[48]. These fusion constructs build on the earlier observation that a class of UDG family members present in fact hypoxanthine-DNA glycosylase activity[50]. Equally consistent with a role for heterochromatin in favouring base editing

through BER inhibition are *in vitro* experiments showing that BER enzymes (e.g., DNA glycosylases, APE1 endonuclease and DNA polymerase β) are substantially more obstructed at chemically modified nucleotides located inward nucleosome surfaces than at the same nucleotides located on more outward positions or naked DNA[51-54]. Significantly, transient DNA unwrapping or directional nucleosome rotations markedly stimulate BER enzymatic activities[51-54]. In line with these results, *in vitro* reconstitution experiments revealed that ATP-dependent chromatin remodelling factors greatly facilitate BER reactions on nucleosome-wrapped DNA[55]. In addition, experiments in cells point to an inverse correlation between the extent of chromatin compaction and BER engagement. In particular, BER complexes assemble preferentially at euchromatic over heterochromatic regions in HeLa cells exposed to base-damaging oxidative stress[56]. It is also noteworthy to mention that, when compared to epigenetically silent loci, open loci greatly facilitate BER initiated by the alkyladenine DNA glycosylase[57], a key enzyme for the removal of bases with aberrant methyl or deoxyinosine/hypoxanthine groups. Collectively, such *in vitro* and *in cellula* datasets suggest that compact chromatin hinders the recruitment and activity of BER enzymes. Hence, in cells, the combined net effects of epigenetically-controlled target DNA accessibility and BER hindrance levels might ultimately determine whether base editing activity is lower, similar or higher at specific sites in open versus closed chromatin (**Supplementary Figure S10**).

Notably, our experiments have further revealed that in addition to base editing frequencies, the buildup of different types of bystander products and their proportions can equally depend on the epigenetic context of target sequences. Bystander effects assessed comprised (i) base editing outside the predefined editing windows of ABE and CBE complexes; and (ii) target-to-unintended base pair conversions. The former and latter byproduct categories define the precision and purity attained by individual base editing complexes, respectively. Besides confirming that ABEs offer substantially higher product purity than CBEs[23], our data suggest that mutagenic translesion synthesis (TLS), a putative source of target-to-unintended CBE products[37], can be contingent upon the epigenetic context of modified bases. Our results further revealed that when compared to ABE complexes, CBE complexes exhibit a higher tendency for base editing "spillover" outside their activity windows upon heterochromatic-to-euchromatic target sequence transitions. As corollary, the activity windows of base editors, in particular CBEs, are not necessarily fixed in that, in addition to specific protein architectures (e.g. effector domains and linker lengths used), they may also depend on extrinsic factors, namely, alternate higher-order chromatin conformations.

In addition to serving as a powerful set of complementary gene-editing tools for basic research, base editors and prime editors constitute high-potential reagents for genetic therapies with base editors having already entered clinical testing[58]. Thus, the performance and safety profiles of these technologies as such or of their individual components in particular (i.e., protein and sequence-specific RNA moieties) necessitates in-depth scrutiny for guiding their selection, further development and application in specific contexts. On the basis of our results, we submit that it will be critical to assess the role of higher-order chromatin environments on the performances of prime editors and base editors as these environments, at both on- and off-target sequences, might vary in different cell types or during the dynamic epigenetic regulation underlying organismal development and cellular differentiation. Furthermore, algorithms trained to predict the activities of DSB-free gene editing reagents, besides target nucleotide sequences per se, will equally profit from processing information on the epigenetic context of said sequences. Finally, our data can further guide the development of combinatorial approaches whereby targeted epigenetic modulators and DSB-free DNA editing tools work in concert for attaining more efficient and/or more precise genomic modifications.

Materials and Methods

Cells

The generation and characterization of the reporter cells HEK.EGFP$^{TetO.KRAB}$ were detailed elsewhere[29]. These cells were kept in high-glucose Dulbecco's modified Eagle's medium (DMEM; Thermo Fisher Scientific; Cat.No.: 41966-029) containing 10% fetal bovine serum (FBS; Biowest; Cat.No.: S1860-500). The generation of the human embryonic retinoblasts HER.TLR$^{TetO.KRAB}$, and of their control *TetO*-negative counterparts HER.TLR^{KRAB}, has also been described before[29]. These cells contain the Traffic Light Reporter (TLR) system[59], and were cultured in DMEM supplemented with 10% FBS and 10 mM $MgCl_2$. The human embryonic kidney 293T (HEK293T) cells (obtained from the American Type Culture

Collection), and their CD81-negative and CD81-positive derivatives obtained by FACS after CRISPRoff-mediated *CD81* silencing were cultured in DMEM containing 10% FBS. All cells used in this study were tested for mycoplasma and were kept in a humidified-air 5% CO_2 atmosphere at 37°C.

Recombinant DNA
Standard molecular cloning methods were applied in this study. The gRNA-expressing constructs were assembled by inserting annealed oligonucleotide pairs listed in **Supplementary Table S1** into BveI-digested AY56_pU6.opt-sgRNA.BveI-stuffer[60] or AZ64_pU6.opt-sgRNA.BveI-stuffer. The generation of pegRNA-expressing constructs was initiated by annealing the corresponding oligonucleotide pairs whose sequences are listed in **Supplementary Table S2**. Afterwards, the annealed oligonucleotide pairs were ligated to BsaI-digested AJ71_pU6.PEgRNA-GG-acceptor (Addgene plasmid #132777). The construct gRNA_GFP-T2[61], herein named AT44_gRNA$^{GFP.T2}$, was obtained from Addgene plasmid #41820. Plasmid AM51_pU6.gRNA-I-SceI[29] encoding an irrelevant, non-targeting, gRNA served as a negative control.

Cell transfections
Cell transfections were carried out using as transfection agent 25-kDa linear polyethyleneimine (PEI; Polysciences; Cat.No.: 23966-1) solution (pH 7.4). Prior to transfection, HEK.EGFP$^{TetO.KRAB}$ cells were cultured for 7 days in the presence or absence of 200 ng ml^{-1} doxycycline (Dox; Clontech; Cat. No.: 8634-1). HER.TLR$^{TetO.KRAB}$ and HER.TLR^{KRAB} cells were instead kept for 10 days in medium with or without 500 ng ml^{-1} Dox prior to transfection. Next, the cells were seeded in the indicated culture vessels (**Supplementary Tables S3**-**S16**) and 16 h to 24 h later, transfections were initiated by mixing the relevant plasmids in a 150 mM NaCl solution to which the appropriate amount of a 1 mg ml^{-1} PEI solution was immediately added. After vigorous shaking with a vortex for about 10 sec, the transfection mixtures were incubated for 15 min at room temperature (RT) with the formed DNA-PEI complexes being then directly added into the culture media of the target cells. At 6 h post-transfection, the transfection media were replaced with regular culture media. The cell numbers, the compositions of each DNA mixture used in the different transfection reactions (in ng), the volumes of 150 mM NaCl and PEI solutions (in μl) are specified in **Supplementary Tables S3**-**S16**.

Flow cytometry analyses
The live-cell quantification of gene-editing events resulting from base editing and prime editing was done by using reporter-directed flow cytometry at the indicated timepoints. The initial transfection efficiencies were measured on a per sample basis at 3 days post-transfection for endpoint normalization of gene-editing frequencies. In brief, transfected cells were washed with phosphate-buffered saline (PBS; pH 7.4; Fresenius Kabi; Cat. No.: 16QI2226) and were then treated with a trypsin-EDTA solution (Thermo Fisher Scientific; Cat. No.: 15400-054) to generate single-cell suspensions. After cell collection by a 5-min centrifugation at 300 ×g, the dissociated cells were resuspended in PBS containing 0.5% bovine serum albumin (BSA; Sigma; Cat. No.: A9647-100G) and 2 mM EDTA (pH 8.0). The detection of fluorescence signals was carried out with the aid of a BD LSR II flow cytometer (BD Biosciences) using the appropriate filters. Background fluorescence thresholds were established by applying parental non-transfected cells as negative controls. At least 10,000 viable single cells were acquired per sample. FlowJo 10.6.0 software (Tree Star) was used for data analyses.

***CD81* epigenetic remodeling**
The CRISPRoff system[36] was exploited to investigate the impact of alternate chromatin states on base-editing and prime-editing activities at the endogenous *CD81* locus. The implementation of the CRISPRoff system was initiated by plating HEK293T cells in wells of 24-well plates at a density of 2.0 x 10^5 cells per well. Approximately 17 h later, the cells were transfected by using PEI with the plasmid mixtures indicated in **Supplementary Table S10** designed for *CD81*-targeted epigenetic silencing. After a 7-day subculturing period, the efficiency of targeted gene silencing induced by CRISPRoff was determined by CD81-directed flow cytometry. In brief, cells were washed with PBS (pH 7.4), and subsequently incubated in trypsin-EDTA to generate single-cell suspensions. After trypsin neutralization, 1×10^5 cells were centrifuged at 300 ×g for 5 min after which the pelleted cells were resuspended in 100 ml of ice-cold PBS supplemented with 2% BSA and 2 ml of phycoerythrin (PE)-conjugated anti-CD81 antibody (BD Pharmingen™; Cat. No.: 555676). The cells were stained on ice for at least 30 min in the dark before being washed thrice with ice-cold PBS containing 1% BSA. The frequencies of CD81-

negative cells were determined via a BD LSR II flow cytometer. Next, the cell populations transfected with the CRISPRoff and gRNA plasmid combination yielding the most robust *CD81* silencing levels were expanded. Next, an Arial III flow cytometer was used to sort CD81-negative and CD81-positive populations. CD81 staining and flow cytometry were also carried out for assessing the phenotypic stability of the CD81-negative cell population at 1, 2, 3, and 4 weeks post-sorting. The transfections of constructs encoding prime-editing and base-editing reagents designed for installing 1-bp substitutions at different *CD81* positions, were performed side-by-side in CD81-negative and CD81-positive cells (**Supplementary Tables S11** and **S16**). The cells were then harvested at 2 days post-transfection for western blot analysis of gene-editing proteins and, at 7 days post-transfection, for amplicon deep sequencing analyses of base editing and prime editing in CD81-negative and CD81-positive HEK293T cells. In parallel, RT-qPCR analysis was used for tracing *CD81* mRNA levels in CD81-negative and CD81-positive HEK293T cell populations.

Western blot analyses

The tracing of prime editor proteins in CD81-negative and CD81-positive HEK293T cells was assessed by western blotting. Briefly, at 48 h post-transfection, cells were directly collected in Laemmli buffer consisting of 8.0% glycerol, 3% sodium dodecyl sulfate (SDS), and 200 mM Tris-HCl (pH 6.8). The resulting cell lysates were then heated at 100°C for 5 min and protein concentrations were determined with the aid of the DC™ protein assay kit (Bio-Rad; Cat. No.: 5000111) following the manufacturer's recommendations. Next, 20-µg protein samples were separated by 6% SDS-polyacrylamide gel electrophoresis (SDS-PAGE) and were subsequently transferred onto 0.45-µm polyvinylidene difluoride (PVDF) membranes. Non-specific antibody binding was blocked by incubating the membranes in 5% (w/v) non-fat dry milk (Campina Elk; Cat. No.: 112349) dissolved in Tris-buffered saline (TBS; 50 mM Tris-HCl pH 7.6; 150 mM NaCl) supplemented with 0.1% (v/v) Tween 20 (Merck Millipore; Cat. No.: 8221840500) (TBST) at RT for at least 1 h. The blocked membranes were immediately incubated with the primary antibodies directed against *S. pyogenes* Cas9 (Abcam; Cat. No.: ab191468) or vinculin (Sigma-Aldrich; Cat. No.: V9131), each diluted 1:1000 in TBST containing 5% BSA. After overnight incubation at 4°C, the membranes were washed thrice with TBST before being exposed to a horseradish peroxidase (HRP)-conjugated secondary antibody directed against mouse IgG (Sigma-Aldrich; Cat. No.: NA931V) diluted 1:5000 in TBST containing 1% non-fat dry milk at RT for 2 h. Clarity™ Western ECL Substrate (Bio-Rad; Cat. No.: 1705060) was applied for signal detection by using the ChemiDoc Imaging System (Bio-Rad).

RT-qPCR analyses

Tracing CRISPRoff-induced *CD81* silencing at the mRNA level was done via RT-qPCR. In brief, total RNA was first extracted from CD81-negative and CD81-positive HEK293T cells by using the NucleoSpin RNA Kit (Macherey-Nagel; Cat. No.: 740955) following the manufacturer's recommendations. Afterwards, equal amounts of isolated RNA templates were applied for reverse transcription with the RevertAid RT Reverse Transcription Kit (Thermo Fisher Scientific; Cat. No.: K1691). In brief, 1 µg of RNA was incubated with 0.5 µl of 100 µM random hexamer primers and 0.5 µl of 100 µM Oligo(dT)$_{18}$ primers in 12 µl reaction volumes at 65°C for 5 min followed by an 2-min incubation at 4°C. Subsequently, 1 µl of 20 U µl^{-1} RiboLock RNase Inhibitor, 1 µl of 200 U µl^{-1} RevertAid H Minus M-MuLV Reverse Transcriptase, 2 µl of 10 mM dNTP Mix and 4 µl of 5× Reaction Buffer, were directly added to each sample and the resulting mixtures were incubated at 25°C for 5 min followed by an 1-h incubation at 42°C. Afterwards, the reverse transcriptase was deactivated by heating the samples at 70°C for 5 min. Next, the resulting cDNA was subjected to qPCR by using the primers listed in **Supplementary Table S17** together with the iQ™ SYBR® Green Supermix (Bio-Rad; Cat. No.: L010171C). The qPCR signals were detected with the aid of a CFX Connect Real-Time PCR Detection System (Bio-Rad). The relative *CD81* mRNA expression was analyzed through the $2^{-\Delta\Delta Ct}$ method with *GAPDH* transcripts serving as internal controls for gene expression normalization. The qPCR cycling conditions and mixture components used for the analysis of *CD81* mRNA expression are specified in **Supplementary Tables S17** and **S18**, respectively.

ChIP-qPCR analyses

Establishing the acquisition of euchromatic and heterochromatic marks at *CD81* alleles was performed via ChIP-qPCR analyses as follows. Briefly, 2×10^7 cells were crosslinked with 1% formaldehyde for 10 min at RT and then immediately quenched with 1.25 M glycine (Thermo Fisher Scientific; Cat. No.:

120070050) for 5 min at RT. Next, the cells were washed twice with ice-cold PBS (pH 7.4) before being lysed in lysis buffer containing 5 mM piperazine-N,N'-bis(2-ethanesulfonic acid) (PIPES; pH 8.0; Sigma; Cat. No.: P6757), 85 mM KCl, 0.5% NP40 (Sigma; Cat. No.: 74385), and 1% proteinase inhibitor cocktail (Roche; Cat. No.: 11849300) for 10 min on ice. After a 5-min centrifugation at 510 ×g at 4°C, the sample supernatants were removed and the resulting nuclei portions were directly subjected to nuclei lysis buffer consisting of 50 mM Tris pH 8.0, 10 mM EDTA, 1% SDS, and 1% proteinase inhibitor cocktail for 10 min on ice. Next, the chromatin was sheared by using a sonication device (Diagenode) set to optimized conditions predefined to obtain DNA fragments spanning the 200-bp to 700-bp range, i.e., 3 sec on, 6 sec off, 30% amplitude for 3 min. The sonicated samples were subsequently centrifuged at 17,949 ×g for 20 min at 4°C, and the resulting supernatants were collected and diluted 5-fold in immunoprecipitation (IP) dilution buffer (50 mM Tris pH 7.5, 150 mM NaCl, 1 mM EDTA, 1% NP40, 0.25% sodium deoxycholate (Sigma; Cat. No.: D6750), and 1% proteinase inhibitor cocktail). A fraction of the cell lysis material (5% of total) corresponding to each sample was saved as input for qPCR normalization. The remaining cell lysis material of each sample was precleared with Protein A/G Sepharose beads (GE Healthcare; Cat. No.: 17-0963-03 or 17-0618-02) and salmon sperm DNA for at least 1 h at 4°C with agitation. Afterwards, immunoprecipitations were carried out by incubating the aforesaid cell lysis materials overnight at 4°C with ChIP-grade antibodies raised against H3K9me3 (10 µg; rabbit; Active Motif; Cat. No.: 39765), H3Ac (10 µg; rabbit; Active Motif; Cat. No.: 61637), RNA Pol II (2.5 µg; mouse; Active Motif; Cat. No.: 39097), IgG (10 µg; rabbit; Cell Signaling Technology; Cat. No.: 2729) or IgG (2.5 µg; mouse; Cell Signaling Technology; Cat. No.: 5415). In parallel, appropriate amounts of Protein A/G Sepharose beads were blocked overnight in 1% BSA. The next day, 100 µl of blocked beads were added to the cell lysis samples. After a 2-h incubation at 4°C with agitation, the beads were harvested and washed by using the following protocol: once with IP wash buffer #1 for 5 min at RT (20 mM Tris pH 8.0, 2 mM EDTA, 50 mM KCl, 1% Triton X-100 (Merck Millipore; Cat. No.: 1086031000), and 0.1% SDS), twice with high salt buffer for 5 min at RT (20 mM Tris pH 8.0, 2 mM EDTA, 500 mM NaCl, 1% Triton X-100, and 0.01% SDS), once with IP wash buffer #2 for 5 min at RT (10 mM Tris pH 8.0, 1 mM EDTA, 0.25 lithium chloride (J.T. Baker; Cat. No.: 0516), 1% NP40, and 1% sodium deoxycholate), and twice with TE buffer #1 for 5 min at RT (10 mM Tris pH 8.0, 1 mM EDTA). After these washing steps, the DNA in the various samples was eluted in elution buffer containing 50 mM sodium bicarbonate and 1% SDS at 65°C for 1 h and the subjected treated with 5 ml of 10 mg ml^{-1} RNase A (Thermo Fisher Scientific; Cat. No.: EN0531) overnight at 37°C, followed by a 5-h incubation with 2.5 ml of 20 mg ml^{-1} proteinase K (Thermo Fisher Scientific; Cat. No.: EO0491) at 55°C. Subsequently, the resulting DNA was precipitated by incubation overnight at -80°C in 500 ml of isopropanol supplemented with 2 ml of 20 mg ml^{-1} glycogen (Thermo Fisher Scientific; Cat. No.: R0551). The DNA pellets were harvested by centrifugation at 17,949 ×g for at least 30 min at 4°C, and were then washed once with 70% ethanol before being dissolved in 100 µl of TE buffer #2 consisting of 1 M Tris pH 8.0, 0.5 M EDTA and 20 mg ml^{-1} RNase A for 1 h at 37°C. Next, 1-µl samples of recovered purified DNA served as template for qPCR quantification by using the iQ™ SYBR® Green Supermix. The primers, cycling conditions and components of the qPCR mixtures are specified in **Supplementary Tables S17 and S18**. Finally, the signal outputs were detected with the aid of a CFX Connect Real-Time PCR Detection System (Bio-Rad).

Deep sequencing analysis

Amplicon deep sequencing was performed for assessing gene editing frequencies and outcomes resulting from the delivery of prime editing and base editing tools into human cells. The HEK.EGFP$^{TetO.KRAB}$ cells were exposed to the transfection mixtures indicated in **Supplementary Tables S11**-**S16**. At 17 days post-transfection, the frequencies of EGFP-negative cells and EBFP-positive cells were determined by flow cytometry as a live-cell readout for gene editing events. In parallel, genomic DNA was extracted with the DNeasy Blood & Tissue kit following the manufacturer's recommendations. Similarly, CD81-negative and CD81-positive HEK293T cells were subjected to prime editing or base editing complexes and, at 10 days post-transfection, genomic DNA was isolated for determining the gene-editing frequencies at the *CD81* locus. In brief, isolated DNA served as template in target-specific PCR mixtures containing Phusion High-Fidelity Polymerase (Thermo Fisher Scientific; Cat. No.: F-530L) and primers possessing adapter tag overhangs. After purification with AMPure XP beads (Beckman Coulter; Cat. No.: A63881), the resulting amplicons were subjected to PCR barcoding using Illumina tag-specific primer pairs possessing unique sequence identifier combinations. The cycling conditions, primer sequences and PCR mixture compositions are specified in **Supplementary Tables S19**-**S23**.

Prior to proceeding with amplicon sample quality control, the barcoded amplicons were purified with AMPure XP beads and their concentrations were measured by using the Qubit dsDNA HS assay kit (Thermo Fisher Scientific; Cat. No.: Q32854) together with a Qubit2.0 fluorometer. Afterwards, amplicon sample quality control was done by capillarity electrophoresis through a 2100 Bioanalyzer system (Agilent) with the Agilent DNA 1000 Kit. Finally, purified amplicons were pooled together in equal molar ratios and were then subjected to Illumina MiSeq deep sequencing for obtaining 50,000 paired-end reads. The paired-end MiSeq raw reads (R1 and R2 fastq files) were subjected to demultiplexing and then analysed with the aid of the CRISPResso2 software[63].

Statistical analyses

GraphPad Prism software (version 8.0.1) was used in the statistical analyses of datasets derived from at least three independent biological replicates. The statistical tests used and resulting significance outputs are, where relevant, indicated in the figures and respective legends.

DATA AVAILABILITY

All data assembled for and analysed in this study are included in the article and supplementary files. The libraries of next-generation sequencing reads are deposited at the NCBI Sequence Read Archive (SRA) database. Any additional information required to reanalyse the data reported in this paper is available from the lead contact upon request.

ACKNOWLEDGMENTS

The authors thank all laboratory members for insightful discussions and members of Leiden Genome Technology Centre and Flow Cytometry Core Facility (Leiden University Medical Center, The Netherlands) for assistance with genomic sequencing and FACS services, respectively. Qian Wang held a Ph.D. fellowship from the China Scholarship Council–Leiden University Joint Scholarship Programme. *Conflict of interest statement*. None declared.

REFERENCES

1. Chen, X., and Gonçalves, M.A.F.V. DNA, RNA, and protein tools for editing the genetic information in human cells. *iScience.* 2018; **6**: 247-263.
2. Cradick, T.J., Fine, E.J., Antico, C.J., and Bao, G. CRISPR/Cas9 systems targeting beta-globin and CCR5 genes have substantial off-target activity. *Nucleic Acids Res.* 2013; **41**: 9584–9592.
3. Fu, Y., Foden, J.A., Khayter, C., Maeder, M.L., Reyon, D., Joung, J.K., and Sander, J.D. High-frequency off-target mutagenesis induced by CRISPR-Cas nucleases in human cells. *Nat. Biotechnol.* 2013; **31**: 822–826.
4. Hsu, P.D., Scott, D.A., Weinstein, J.A., Ran, F.A., Konermann, S., Agarwala, V., Li, Y., Fine, E.J., Wu, X., Shalem, O., et al. DNA targeting specificity of RNA-guided Cas9 nucleases. *Nat. Biotechnol.* 2013; **31**: 827–832.
5. Pattanayak, V., Lin, S., Guilinger, J.P., Ma, E., Doudna, J.A., and Liu D.R. High-throughput profiling of off-target DNA cleavage reveals RNA-programmed Cas9 nuclease specificity. *Nat. Bioatechnol.* 2013; **31**: 839–843.
6. Frock, R.L., Hu, J., Meyers, R.M., Ho, Y.J., Kii, E., and Alt F.W. Genome-wide detection of DNA double-stranded breaks induced by engineered nucleases. *Nat. Biotechnol.* 2015; **33**: 179–186.
7. Chen, X., Tasca, F., Wang, Q., Liu, J., Janssen, J.M., Brescia, M.D., Bellin, M., Szuhai, K., Kenrick, J., Frock, R.L., et al. Expanding the editable genome and CRISPR-Cas9 versatility using DNA cutting-free gene targeting based on in trans paired nicking. *Nucleic Acids Res.* 2020; **48**: 974-995.
8. Wang, Q., Liu, J., Janssen, J.M., Le Bouteiller, M., Frock, R.L., and Gonçalves, M.A.F.V. Precise and broad scope genome editing based on high-specificity Cas9 nickases. *Nucleic Acids Res.* 2021; **49**: 1173–1198.
9. Liu, M., Zhang, W., Xin, C., Yin, J., Shang, Y., Ai, C., Li, J., Meng, F.L., and Hu, J. Global detection of DNA repair outcomes induced by CRISPR-Cas9. *Nucleic Acids Res.* 2021; **49**: 8732-8742.
10. Turchiano, G., Andrieux, G., Klermund, J., Blattner, G., Pennucci, V., El Gaz, M., Monaco, G., Poddar, S., Mussolino, C., Cornu, T.I., et al. Quantitative evaluation of chromosomal rearrangements in gene-edited human stem cells by CAST-Seq. *Cell Stem Cell.* 2021; **28**: 1136–1147.

11. Kosicki, M., Tomberg, K., and Bradley, A. Repair of double-strand breaks induced by CRISPR-Cas9 leads to large deletions and complex rearrangements. *Nat. Biotechnol.* 2018; **36**: 765–771.
12. Boutin, J., Rosier, J., Cappellen, D., Prat, F., Toutain, J., Pennamen, P., Bouron, J., Rooryck, C., Merlio, J.P., Lamrissi-Garcia, I., et al. CRISPR-Cas9 globin editing can induce megabase-scale copy-neutral losses of heterozygosity in hematopoietic cells. *Nat. Commun.* 2021; **12**: 4922.
13. Leibowitz, M.L., Papathanasiou, S., Doerfler, P.A., Blaine, L.J., Sun, L., Yao, Y., Zhang, C.Z., Weiss, M.J., and Pellman, D. Chromothripsis as an on-target consequence of CRISPR-Cas9 genome editing. *Nat. Genet.* 2021; **53**:895-905.
14. Nahmad, A.D., Reuveni, E., Goldschmidt, E., Tenne, T., Liberman, M., Horovitz-Fried, M., Khosravi, R., Kobo, H., Reinstein, E., Madi, A., et al. Frequent aneuploidy in primary human T cells after CRISPR-Cas9 cleavage. *Nat. Biotechnol.* 2020; **40**: 1807-1813.
15. Kleinstiver, B.P., Pattanayak, V., Prew, M.S., Tsai, S.Q., Nguyen, N.T., Zheng, Z., and Joung, J.K. High-fidelity CRISPR-Cas9 nucleases with no detectable genome-wide off-target effects *Nature*. 2016; **529**: 490-495.
16. Slaymaker, I.M., Gao, L., Zetsche, B., Scott, D.A., Yan, W.X., and Zhang, F. Rationally engineered Cas9 nucleases with improved specificity. *Science*. 2016; **351**: 84-88.
17. Chen, X., Janssen, J.M., Liu, J., Maggio, I., Jong, A.E.J., Mikkers, H.M.M., and Gonçalves, M.A.F.V. In trans paired nicking triggers seamless genome editing without double-stranded DNA cutting. *Nat. Commun.* 2017; **8**: 657.
18. Nakajima, K., Zhou, Y., Tomita, A., Hirade, Y., Gurumurthy, C.B., and Nakada, S. Precise and efficient nucleotide substitution near genomic nick via noncanonical homology-directed repair. *Genome Res.* 2018; **28**: 223–230.
19. Hyodo, T., Rahman, M.L., Karnan, S., Ito, T., Toyoda, A., Ota, A., Wahiduzzaman, M., Tsuzuki, S., Okada, Y., Hosokawa, Y., et al. Tandem paired nicking promotes precise genome editing with scarce interference by p53. *Cell Rep.* 2020; **30**: 1195–1207.
20. Bollen, Y., Hageman, J.H., van Leenen, P., Derks, L.L.M., Ponsioen, B., Buissant des Amorie, J.R., Verlaan-Klink, I., van den Bos, M., Terstappen, L.W.M.M., van Boxtel, R., et al. Efficient and error-free fluorescent gene tagging in human organoids without double-strand DNA cleavage. *PLoS Biol.* 2022; **20**:e3001527.
21. Komor, A.C., Kim, Y.B., Packer, M.S., Zuris, J.A., and Liu, D.R. Programmable editing of a target base in genomic DNA without double-stranded DNA cleavage. *Nature*. 2016; **533**: 420-424.
22. Nishida, K., Arazoe, T., Yachie, N., Banno, S., Kakimoto, M., Tabata, M., Mochizuki, M., Miyabe, A., Araki, M., Hara, K.Y., et al. Targeted nucleotide editing using hybrid prokaryotic and vertebrate adaptive immune systems. *Science*. 2016; **353**: p. aaf8729.
23. Gaudelli, N.M., Komor, A.C., Rees, H.A., Packer, M.S., Badran, A.H., Bryson, D.I., and Liu, D.R. Programmable base editing of A*T to G*C in genomic DNA without DNA cleavage. *Nature*. 2017; **551**: 464-471.
24. Jeong, Y.K., Song, B., and Bae, S. Current Status and Challenges of DNA Base Editing Tools. *Mol. Ther.* 2020; **28**:1938-1952.
25. Anzalone, A.V., Randolph, P.B., Davis, J.R., Sousa, A.A., Koblan, L.W., Levy, J.M., Chen, P.J., Wilson, C., Newby, G.A., Raguram, A., et al. Search-and-replace genome editing without double-strand breaks or donor DNA. *Nature*, 2019; **576**: 149–157.
26. Chen, P.J., Hussmann, J.A., Yan, J., Knipping, F., Ravisankar, P., Chen, P.F., Chen, C., Nelson, J.W., Newby, G.A., Sahin, M., et al. Enhanced prime editing systems by manipulating cellular determinants of editing outcomes. *Cell*. 2021; **184**: 5635-5652.e29.
27. Wang, Q., Liu, J., Janssen, J.M., Tasca, F., Mei, H., and Gonçalves, M.A.F.V. Broadening the reach and investigating the potential of prime editors through fully viral gene-deleted adenoviral vector delivery. *Nucleic Acids Res.* 2021; **49**:11986-12001.
28. Ferreira da Silva, J., Oliveira, G.P., Arasa-Verge, E.A., Kagiou, C., Moretton, A., Timelthaler, G., Jiricny, J., and Loizou, J.I. Prime editing efficiency and fidelity are enhanced in the absence of mismatch repair. *Nat. Commun.* 2020; **13**: 760.
29. Chen, X., Rinsma, M., Janssen, J.M., Liu, J., Maggio, I., and Gonçalves, M.A.F.V. Probing the impact of chromatin conformation on genome editing tools. *Nucleic Acids Res*. 2016; **44**: 6482-92.
30. Dear, R.M., Cutts, J.P., Brafman, D.A., and Haynes, K.A. The impact of chromatin dynamics on Cas9-mediated genome editing in human cells. *ACS Synth. Biol.* 2017; **6**:428-438.

31. Chen, X., Liu, J., Janssen, J.M., and Gonçalves, M.A.F.V. The Chromatin Structure Differentially Impacts High-Specificity CRISPR-Cas9 Nuclease Strategies. *Mol. Ther. Nucleic Acids*. 2017; **8**: 558-563.
32. Jensen, K.T., Fløe, L., Petersen, T.S., Huang, J., Xu, F., Bolund, L., Luo, Y., and Lin, L. Chromatin accessibility and guide sequence secondary structure affect CRISPR-Cas9 gene editing efficiency. *FEBS Lett.* 2017; **591**:1892-1901.
33. Urrutia, R. KRAB-containing zinc-finger repressor proteins. *Genome Biol,* 2003; **4**: 231.
34. Szulc, J., Wiznerowicz, M., Sauvain, M.O., Trono, D., and Aebischer P. (2006) A versatile tool for conditional gene expression and knockdown. *Nat. Methods*. 2006; **3**: 109-116.
35. Groner, A.C., Meylan, S., Ciuffi, A., Zangger, N., Ambrosini, G., Dénervaud, N., Bucher, P., and Trono, D. KRAB-zinc finger proteins and KAP1 can mediate long-range transcriptional repression through heterochromatin spreading. *PLoS Genet*. 2010; **6**, e1000869.
36. Nuñez, J.K., Chen, J., Pommier, G.C., Cogan, J.Z., Replogle, J.M., Adriaens, C., Ramadoss, G.N., Shi, Q., Hung, K.L., Samelson, A.J., et al. Genome-wide programmable transcriptional memory by CRISPR-based epigenome editing. *Cell*. 2021; **184**: 2503-2519.
37. Jiang, G., Wang, J., Zhao, D., Chen, X., Pu, S., Zhang, C., Li, J., Li, Y., Yang, J., Li, S., et al. Molecular mechanism of the cytosine CRISPR base editing process and the roles of translesion DNA polymerases. *ACS Synth. Biol.* 2021; **10**: 3353-3358.
38. Park, S.J., Jeong, T.Y., Shin, S.K., Yoon, D.E., Lim, S.Y., Kim, S.P., Choi, J., Lee, H., Hong, J.I., Ahn, J., et al. Targeted mutagenesis in mouse cells and embryos using an enhanced prime editor. *Genome Biol.* 2021; **22**: 170.
39. Chen, R., Cao, Y., Liu, Y., Zhao, D., Li, J., Cheng, Z., Bi, C., and Zhang, X. Enhancement of a prime editing system via optimal recruitment of the pioneer transcription factor P65. *Nat. Commun.* 2023; **14**: 257.
40. Nelson, J.W., Randolph, P.B., Shen, S.P., Everette, K.A., Chen, P.J., Anzalone, A.V., An, M., Newby, G.A., Chen, J.C., Hsu, A. et al. Engineered pegRNAs improve prime editing efficiency. *Nat. Biotechnol.* 2022; **40**, 402-410.
41. Richter, M.F., Zhao, K.T., Eton, E., Lapinaite, A., Newby, G.A., Thuronyi, B.W., Wilson, C., Koblan, L.W., Zeng, J., Bauer, D.E., et al. Phage-assisted evolution of an adenine base editor with improved Cas domain compatibility and activity. *Nat. Biotechnol.* 2020; **38**: 883-891.
42. Koblan, L.W., Doman, J.L., Wilson, C., Levy, J.M., Tay, T., Newby, G.A., Maianti, J.P., Raguram, A., and Liu, D.R. Improving cytidine and adenine base editors by expression optimization and ancestral reconstruction. *Nat. Biotechnol*. 2018; *36*: 843-846.
43. Yang, C., Dong, X., Ma, Z., Li, B., Bi, C., and Zhang, X. Pioneer Factor Improves CRISPR-Based C-To-G and C-To-T Base Editing. *Adv. Sci. (Weinh)*. 2022; **9**: e2202957.
44. Yang, C., Ma, Z., Wang, K., Dong, X., Huang, M., Li, Y., Zhu, X., Li, J., Cheng, Z., Bi, C., and Zhang, X. HMGN1 enhances CRISPR-directed dual-function A-to-G and C-to-G base editing. *Nat. Commun.* 2023; **14**: 2430.
45. Shin, H.R., See, J.E., Kweon, J., Kim, H.S., Sung, G.J., Park, S., Jang, A.H., Jang, G., Choi, K.C., Kim, I., Kim, J.S., and Kim, Y. Small-molecule inhibitors of histone deacetylase improve CRISPR-based adenine base editing. *Nucleic Acids Res*. 2021; **49**: 2390-2399.
46. Liu, N., Zhou, L., Lin, G., Hu, Y., Jiao, Y., Wang, Y., Liu, J., Yang, S., and Yao, S. HDAC inhibitors improve CRISPR-Cas9 mediated prime editing and base editing. *Mol. Ther. Nucleic Acids.* 2022; **29**: 36-46.
47. Roos, W.P., and Krumm, A. The multifaceted influence of histone deacetylases on DNA damage signalling and DNA repair. *Nucleic Acids Res*. 2016; **44**: 10017-10030.
48. Winter, J., Luu, A., Gapinske, M., Manandhar, S., Shirguppe, S., Woods, W.S., Song, J.S., and Perez-Pinera, P. Targeted exon skipping with AAV-mediated split adenine base editors. *Cell Discov*. 2019; **5**: 41.
49. Song, M., Kim, H.K., Lee, S., Kim, Y., Seo, S.Y., Park, J., Choi, J.W., Jang, H., Shin, J.H., Min, S., et al. Sequence-specific prediction of the efficiencies of adenine and cytosine base editors. *Nat. Biotechnol*. 2020; **38**: 1037-1043.
50. Lee, H.W., Dominy, B.N., and Cao, W. New family of deamination repair enzymes in uracil-DNA glycosylase superfamily. *J. Biol. Chem*. 2011; **286**: 31282-7.
51. Beard, B.C., Wilson, S.H., and Smerdon, M.J. Suppressed catalytic activity of base excision repair enzymes on rotationally positioned uracil in nucleosomes. *Proc. Natl. Acad. Sci. USA.* 2003; **100**: 7465–7470.
52. Hinz, J.M., Rodriguez, Y., and Smerdon, M.J. Rotational dynamics of DNA on the nucleosome surface markedly impact accessibility to a DNA repair enzyme. *Proc. Natl. Acad. Sci. USA.* 2010; **107**: 4646–4651.
53. Rodriguez, Y., and Smerdon, M.J. The structural location of DNA lesions in nucleosome core particles determines accessibility by base excision repair enzymes. *J. Biol. Chem*. 2013; **288**: 13863-13875.
54. Hinz, J.M. Impact of abasic site orientation within nucleosomes on human APE1 endonuclease activity. *Mutat Res.* 2014; **766–767**: 19–24.

55. Menoni, H., Gasparutto, D., Hamiche, A., Cadet, J., Dimitrov, S., Bouvet, P., and Angelov, D. ATP-dependent chromatin remodeling is required for base excision repair in conventional but not in variant H2A Bbd nucleosomes. *Mol. Cell Biol*. 2007; **27**: 5949–5956.
56. Amouroux, R., Campalans, A., Epe, B., and Radicella, J.P. Oxidative stress triggers the preferential assembly of base excision repair complexes on open chromatin regions. *Nucleic Acids Res.* 2010; **38**: 2878-2890.
57. Montaldo, N.P., Bordin, D.L., Brambilla, A., Rösinger, M., Fordyce Martin, S.L., Bjørås, K.Ø., Bradamante, S., Aas, P.A., Furrer, A., Olsen, L.C., et al. Alkyladenine DNA glycosylase associates with transcription elongation to coordinate DNA repair with gene expression. *Nat. Commun.* 2019; **10**: 5460.
58. Kingwell, K. Base editors hit the clinic. *Nat. Rev. Drug Discov*. 2022; **21**: 545-547.
59. Certo, M.T., Ryu, B.Y., Annis, J.E., Garibov, M., Jarjour, J., Rawlings, D.J., and Scharenberg, A.M.. Tracking genome engineering outcome at individual DNA breakpoints. *Nat. Methods*. 2011; **8**: 671-676.
60. Maggio, I., Zittersteijn, H.A., Wang, Q., Liu, J., Janssen, J.M., Ojeda, I.T., van der Maarel, S.M., Lankester, A.C., Hoeben, R.C., and Gonçalves, M.A.F.V. Integrating gene delivery and gene-editing technologies by adenoviral vector transfer of optimized CRISPR-Cas9 components. *Gene Ther*. 2020; **27**: 209-225.
61. Mali, P., Yang, L., Esvelt, K.M., Aach, J., Guell, M., DiCarlo, J.E., Norville, J.E., and Church, G.M. RNA-guided human genome engineering via Cas9. *Science*. 2013; **339**: 823-826.
62. Zafra, M.P., Schatoff, E.M., Katti, A., Foronda, M., Breinig, M., Schweitzer, A.Y., Simon, A., Han, T., Goswami, S., Montgomery, E., et al. Optimized base editors enable efficient editing in cells, organoids and mice. *Nat. Biotechnol*. 2018; **36**: 888-893.
63. Clement, K., Rees, H., Canver, M.C., Gehrke, J.M., Farouni, R., Hsu, J.Y., Cole, M.A., Liu, D.R., Joung, J.K., Bauer, D.E., et al. CRISPResso2 provides accurate and rapid genome editing sequence analysis. *Nat. Biotechnol*. 2019; **37**: 224-226.

SUPPLEMENTARY FIGURES

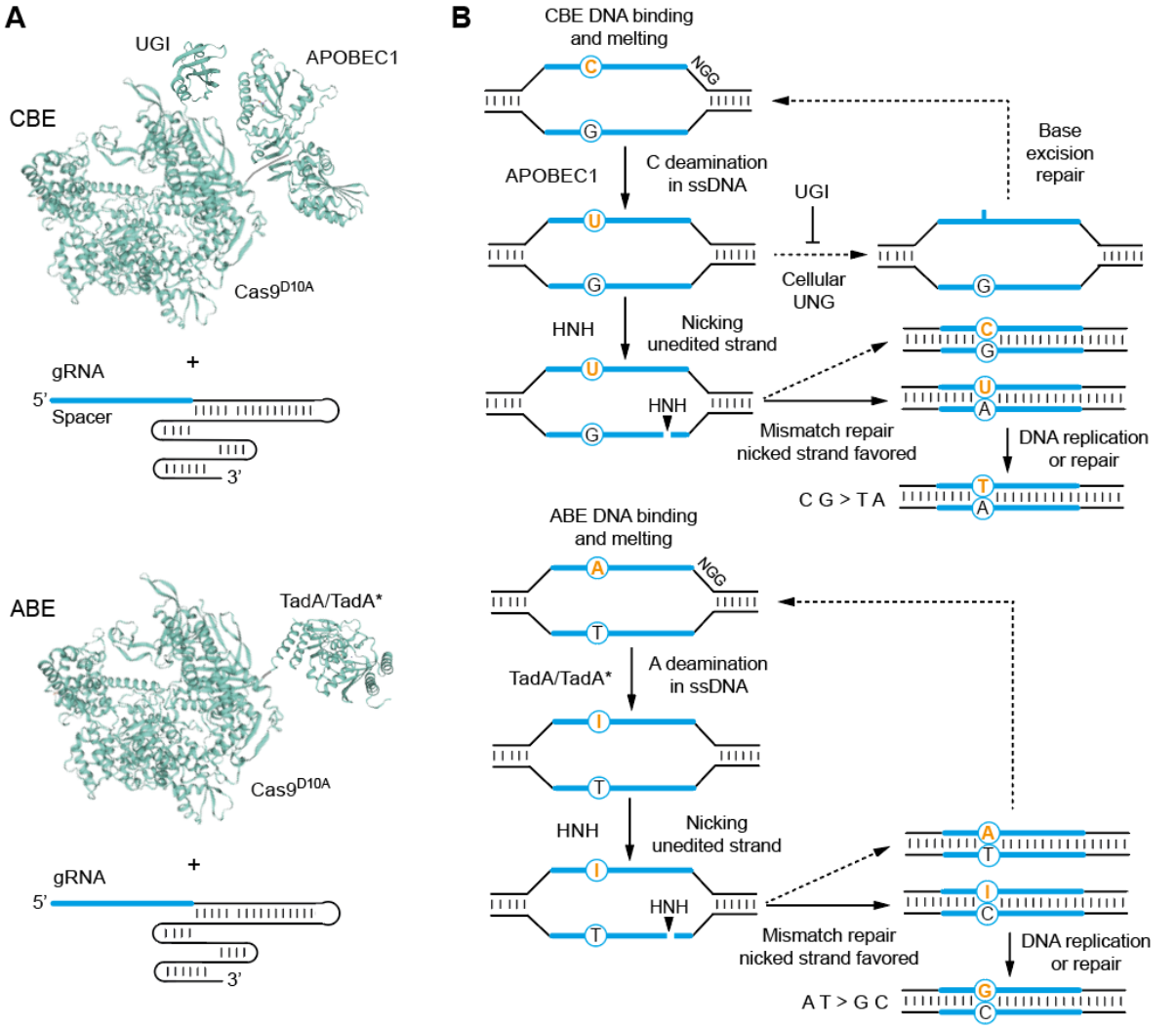

Supplementary Figure S1. Base editing systems. (A) Base editing elements. Cytosine base editors (CBEs) yield C•G to T•A substitutions and are formed by the fusion of a $Cas9^{D10A}$ nickase to a cytosine deaminase, often APOBEC1, and an uracil DNA

glycosylase inhibitor (UGI). Adenine base editors (ABEs) yield A•T to G•C substitutions and are formed by the fusion of a $Cas9^{D10A}$ nickase to an engineered *Escherichia coli* adenine deaminase consisting of a TadA-TadA* heterodimer. In *E. coli* TadA forms a homodimer. One monomer converts adenine to inosine (I) in tRNA and the other assists in substrate binding. In ABEs, the non-catalytic wild-type TadA aids instead an evolved TadA* monomer in catalysing adenine deamination in single-stranded DNA instead of RNA. Both base editor types are addressed to target sequences through a regular gRNA. **(B)** Cytosine and adenine base editing *modus operandi*. CBE:gRNA binding to the target sequence forms an R loop exposing a region of single-stranded DNA. Cs in this single-stranded protospacer bubble become targets for the cytosine deaminase and convert into Us, especially those found in the so-called "activity window" whose position and length depends on the specific base editor architecture. The counterproductive activity of cellular uracil *N*-glycosylases (UNGs) involved in base excision repair of U•G intermediates is inhibited through the UGI moiety. Subsequently, nicking of the strand containing the original G induces cellular mismatch repair of this unedited stand resulting in G-to-A replacement. Finally, upon DNA repair or replication, conversion of the initial C•G into T•A, is completed. ABE:gRNA complexes trigger a series of DNA processing steps similar to those induced by CBE:gRNA complexes except that, upon R loop formation, As exposed in the single-strand DNA bubbles are deaminated by TadA-TadA* to I intermediates. These intermediates are subsequently converted into Cs through DNA repair or replication.

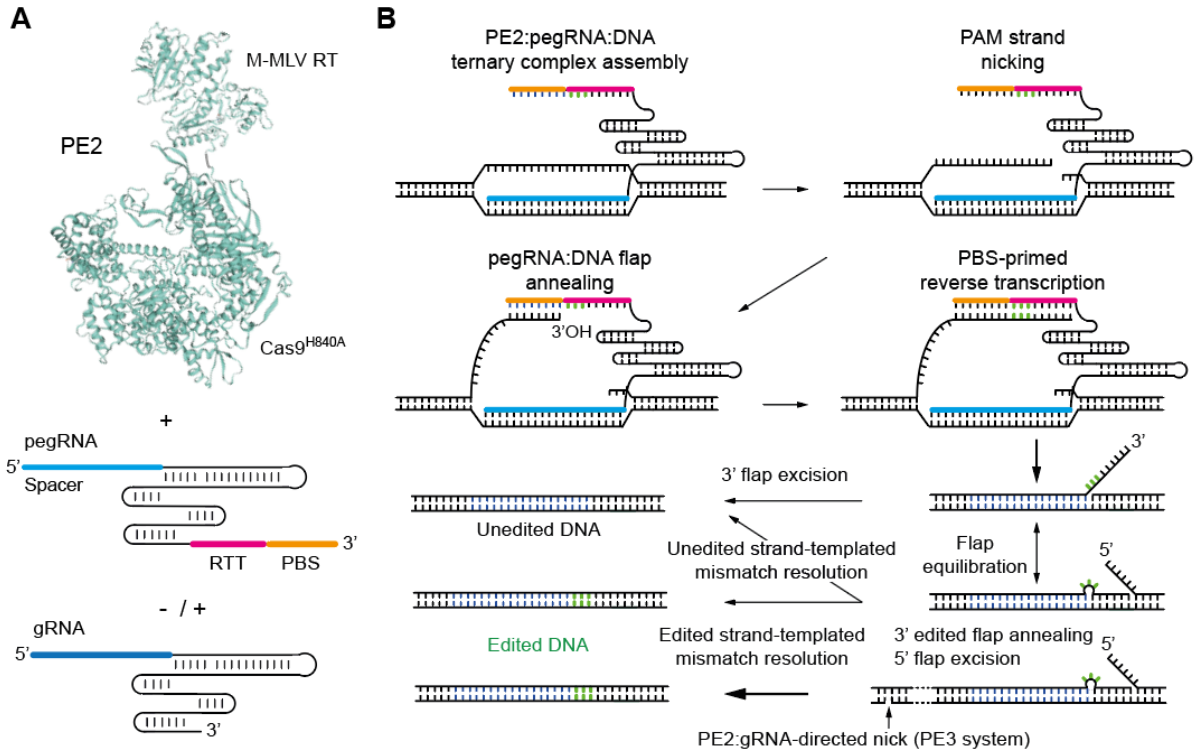

Supplementary Figure S2. Prime editing systems. (A) Prime editing elements. Prime editors are ribonucleoprotein complexes formed by a PE2 protein and a prime editor gRNA (pegRNA). The former element is a fusion product between the $Cas9^{H840A}$ nickase and an engineered Moloney murine leukemia virus reverse transcriptase (M-MLV RT); the latter element is a gRNA extended at the 3' end with reverse transcriptase template (RTT) and primer binding site (PBS) sequences. PE2:pegRNA complexes form the PE2 system. The addition of an auxiliary gRNA forms the PE3 system that can enhance prime editing activities, albeit with increases risks for bystander DSB-induced indel formation resulting from coordinated nicking of both DNA strands. **(B)** Prime editing *modus operandi*. The PE2 protein is addressed to a target sequence through the spacer portion of a pegRNA (PE2 protein not drawn for clarity). At the target site, site-specific nicking releases a single-stranded DNA flap that, after hybridizing to the complementary PBS, provides a free 3'-OH group for M-MLV RT-mediated RNA-dependent DNA polymerization (reverse transcription) over the edit-encoding RTT sequence. Hybridization of the *de novo* synthesized cDNA strand to complementary target DNA and excision of the resulting 5' flap forms heteroduplexes containing edited and unedited strands whose mismatches are further processed to yield edited and unedited homoduplexes. A gRNA directing non-edited strand nicking working in concert with a PE2:pegRNA complex (PE3 system) can enhance the accumulation of the desired edited homoduplexes, presumably through guiding DNA mismatch repair.

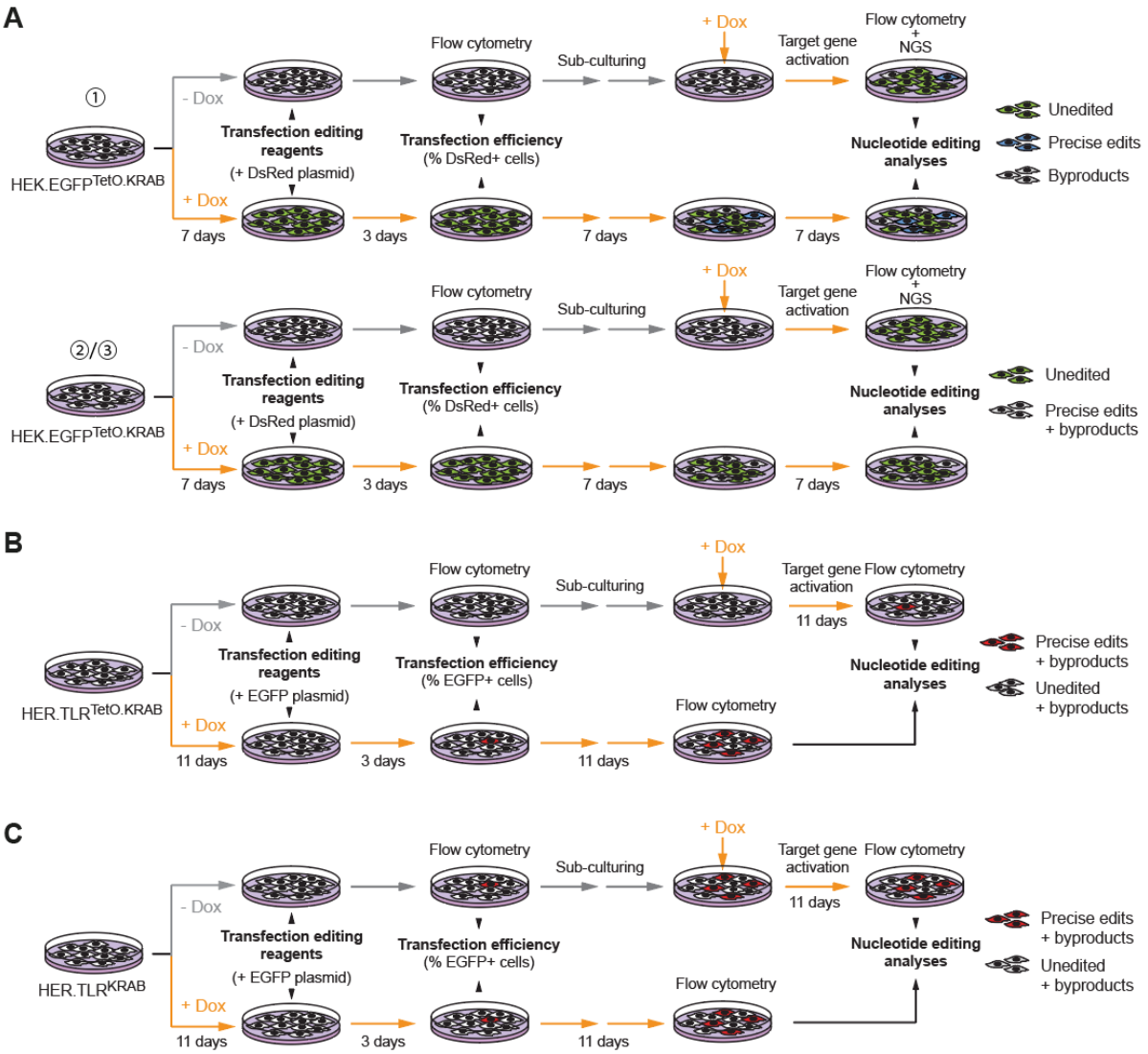

Supplementary Figure S3. Detailed schematics and time courses of DNA editing experiments. The tTR-KRAB-expressing reporter cells HEK.EGFP$^{TetO.KRAB}$ **(A)** and HER.TLR$^{TetO.KRAB}$ **(B)** were used for tracking and quantifying DNA editing outcomes induced by PE2, PE3, CBE and ABE reagents at euchromatic versus heterochromatic nucleotide sequences. The TetO-negative and tTR-KRAB-expressing reporter cells HER.TLR^{KRAB} **(C)** provided for negative controls. The HEK.EGFP$^{TetO.KRAB}$ and HER.TLR$^{TetO.KRAB}$ systems permit assessing DNA editing settings resulting in both gain-of-function and loss-of-functions phenotypes as indicated. The initial higher-order chromatin conformation of target sites in both model alleles is controlled through Dox-dependent regulation of tTR-KRAB binding. HEK.EGFP$^{TetO.KRAB}$ and HER.TLR$^{TetO.KRAB}$ cells with target sites in a heterochromatic (–Dox) or euchromatic (+Dox) state, are transiently transfected with different gene editing constructs. DsRed and EGFP expression plasmids included in the transfection mixtures permit determining transient transfection efficiencies. After the completion of the various nucleotide editing processes in each of the two parallel experimental settings (i.e., –Dox and +Dox), target gene expression is activated allowing quantifying the frequencies of precise and bystander gene editing events flow cytometry and next generation sequencing.

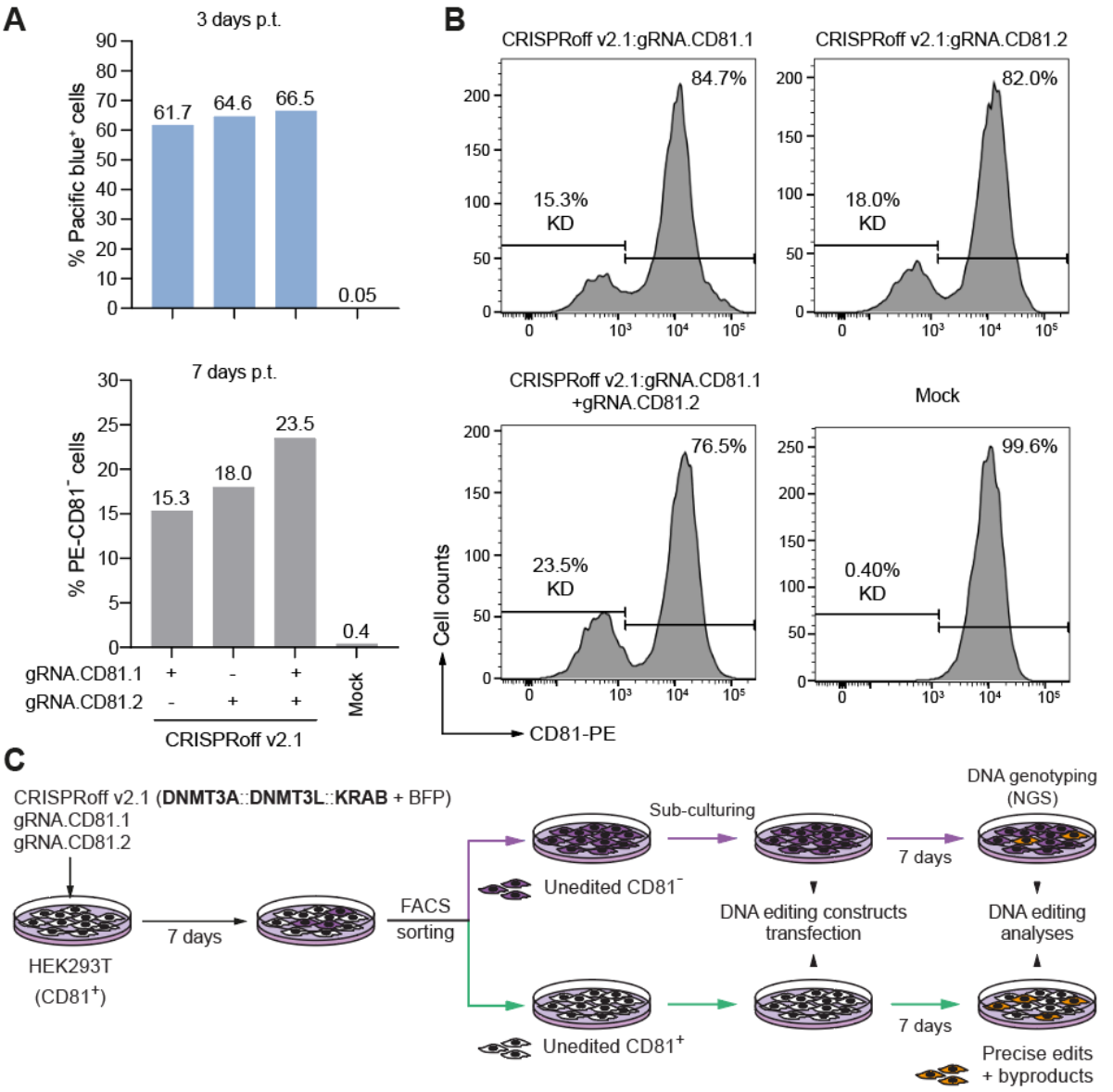

Supplementary Figure S4. Experimental set-up to investigate prime editing and base editing at endogenous sequences in open and close chromatin. (**A**) Epigenetic silencing of *CD81* alleles. HEK293T cells transfected with the indicated combinations of CRISPRoff and gRNA constructs were analysed by flow cytometry for BFP and CD81 expression at 3 and 7 days post-transfection, respectively. The CRISPRoff construct encodes the live-cell reporter BFP and a covalent protein assembly consisting of the DNA methyltransferases DNMT3A and DNMT3L fused to a chromatin remodelling KRAB domain. (**B**) Flow cytometry histograms corresponding to the data depicted in the bottom graph of panel A. (**C**) Diagram and time course of *CD81* gene editing experiments. HEK293T cell populations with *CD81* sequences in epigenetically native and silenced states generated through CRISPRoff transfection and fluorescence activated cell sorting (FACS) of $CD81^-$ and $CD81^+$ cell fractions.

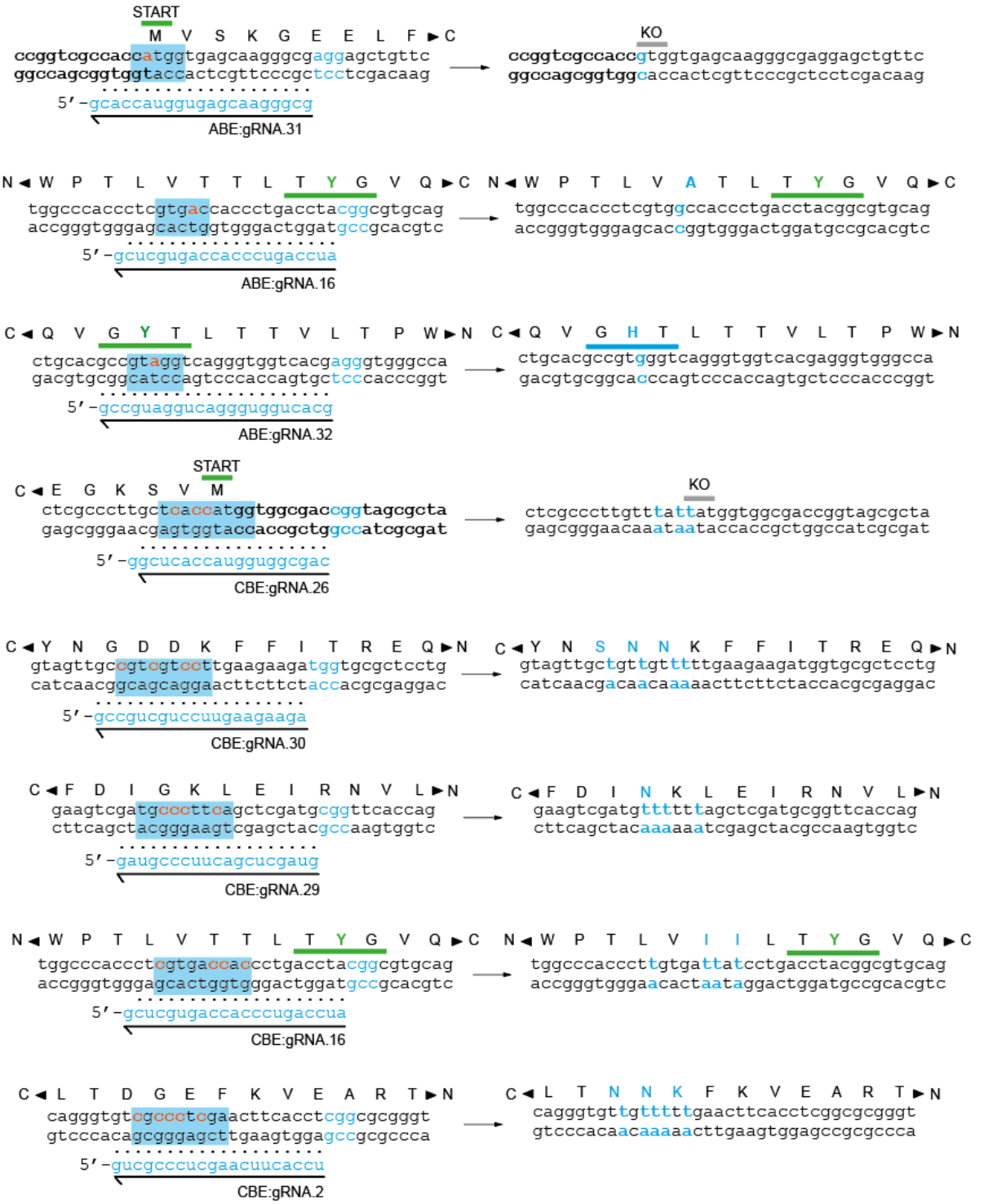

Supplementary Figure S5. Base editing complexes tested in HEK.EGFP$^{TetO.KRAB}$ system. Spacer sequences of gRNAs (horizontal arrows) used in base editing experiments (**Figure 6**) are drawn in relation to their target sites formed by protospacer and NGG PAM sequences. Substrate nucleotides and product base pairs predicted to result from base editing reactions, are highlighted in red and cyan lettering, respectively. Expected base editing windows of and amino acid changes induced by base editors are marked in cyan. EGFP and EBFP fluorophore sequences are underlined in green and cyan, respectively.

EGFP-targeting ABE:gRNA complexes

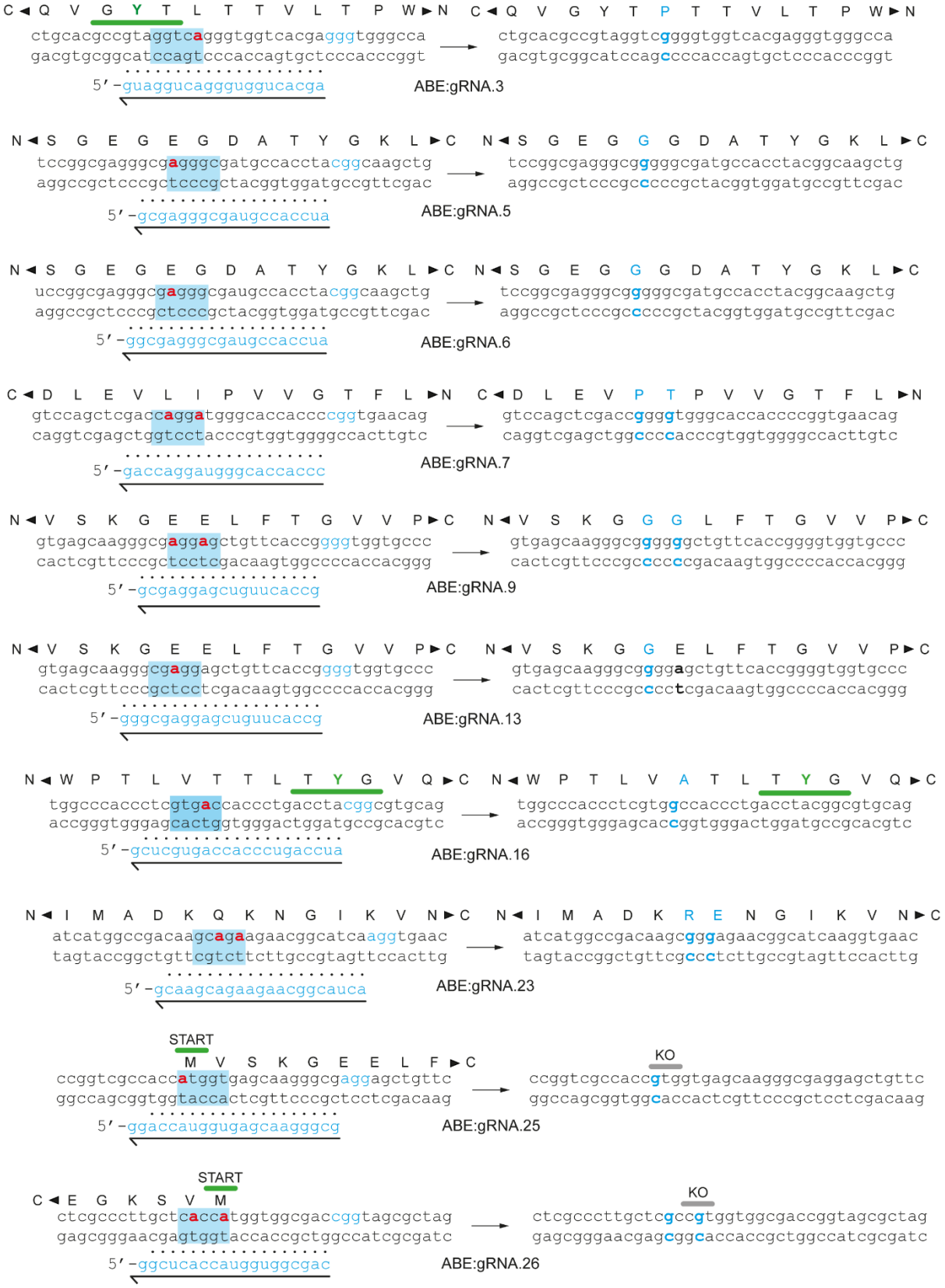

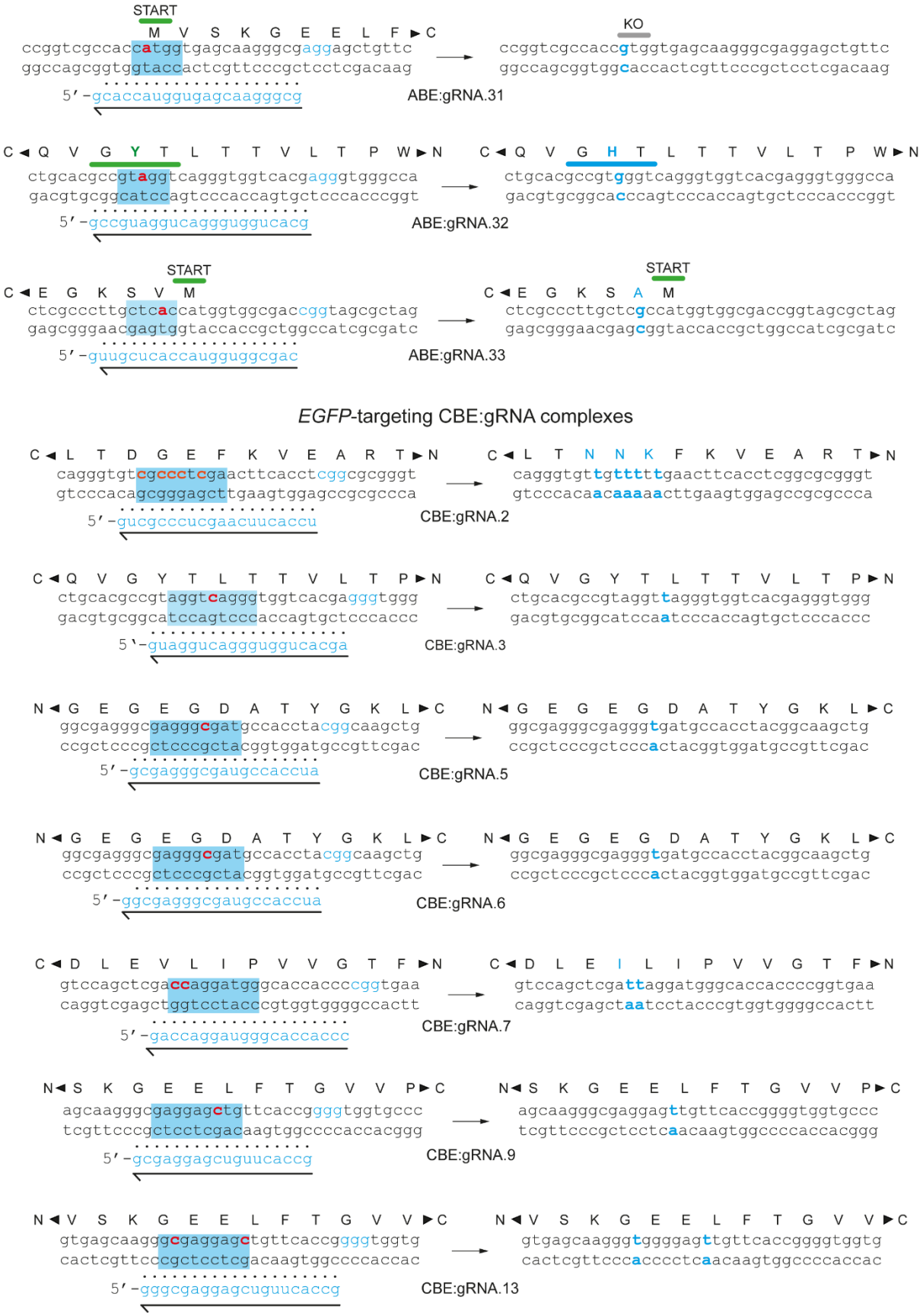
START
KO
ABE:gRNA.31
ABE:gRNA.32
START
START
ABE:gRNA.33
EGFP-targeting CBE:gRNA complexes
CBE:gRNA.2
CBE:gRNA.3
CBE:gRNA.5
CBE:gRNA.6
CBE:gRNA.7
CBE:gRNA.9
CBE:gRNA.13

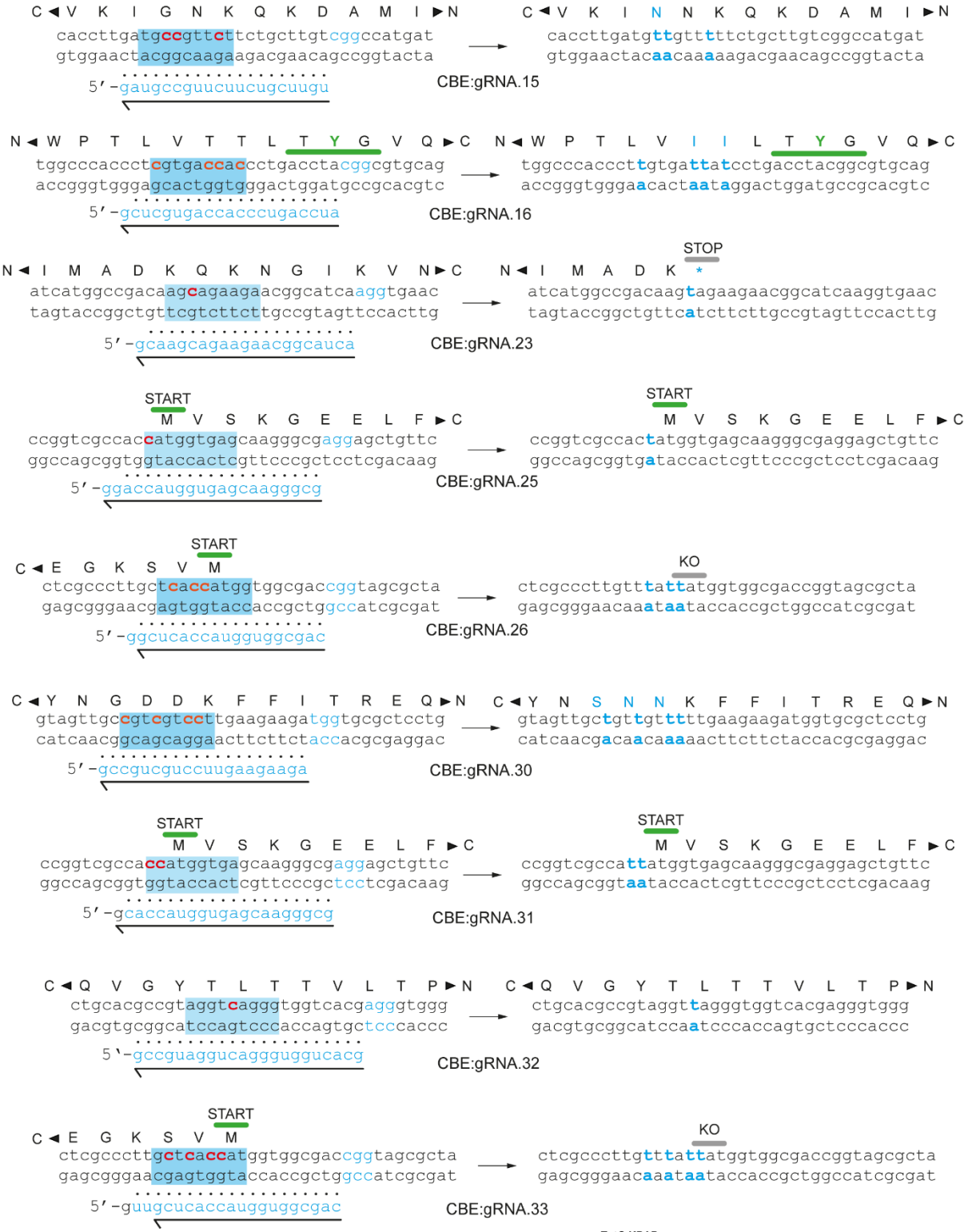

Supplementary Figure S6. Base editing complexes tested in HEK.EGFP$^{TetO.KRAB}$ system. Spacer sequences of gRNAs (horizontal arrows) used in base editing experiments (**Figure 7**) are drawn in relation to their target sites formed by protospacer and NGG PAM sequences. Substrate nucleotides and product base pairs predicted to result from base editing reactions, are highlighted in red and cyan lettering, respectively. Expected base editing windows of and amino acid changes induced by base editors are marked in cyan. EGFP and EBFP fluorophore sequences are underlined in green and cyan, respectively.

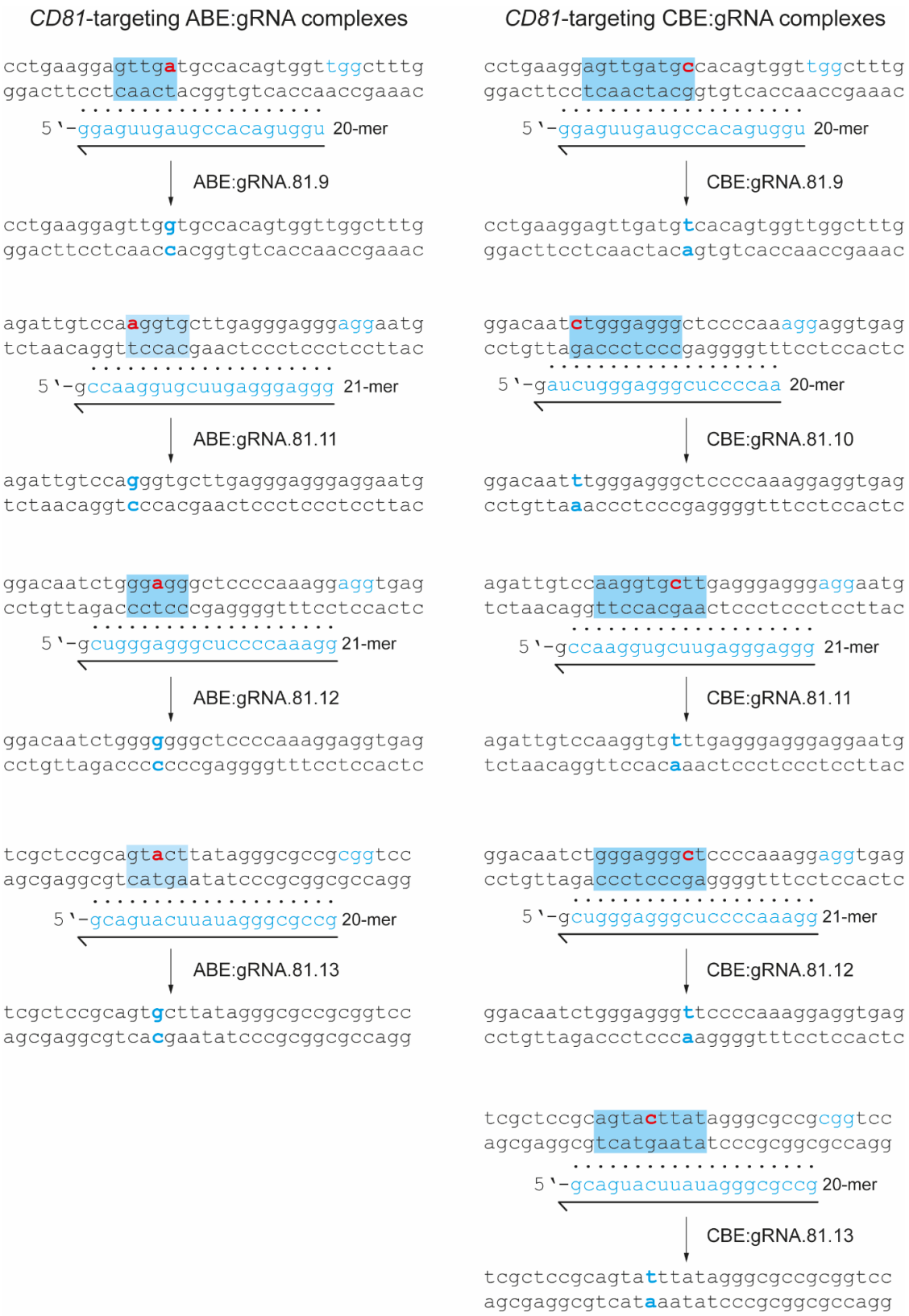

Supplementary Figure S7. Base editing complexes tested in heritable CD81^{+}/CD81^{-} HEK293T cell system. Spacer sequences of gRNAs (horizontal arrows) used in base editing experiments are drawn in relation to their target sites formed by protospacer and NGG PAM sequences. Substrate nucleotides and product base pairs predicted to result from base editing reactions, are highlighted in red and cyan lettering, respectively. Expected base editing windows of and amino acid changes induced by base editors are marked in cyan.

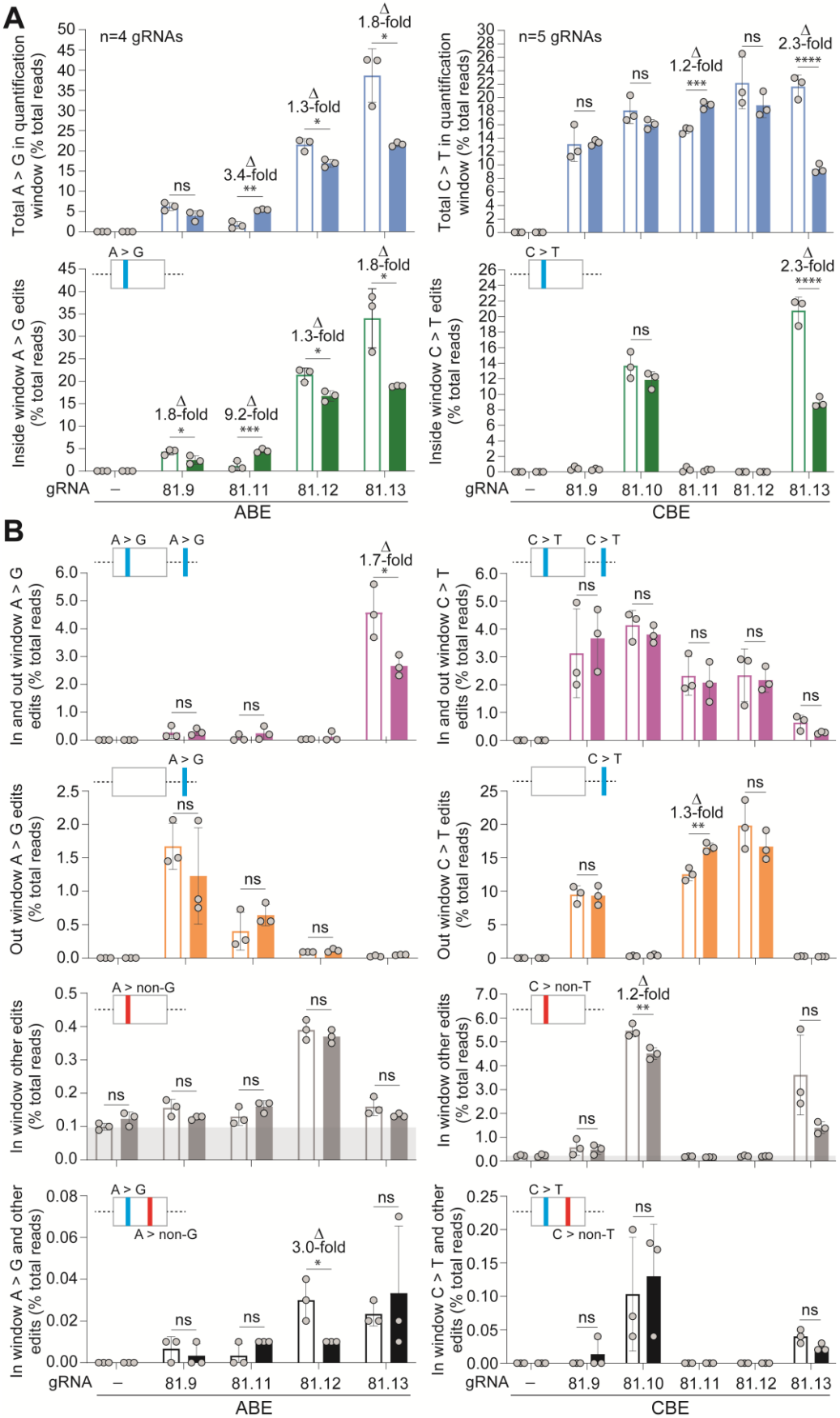

Supplementary Figure S8. Base editing at open and heritable closed chromatin. (**A**) Quantification of base edits at open and closed chromatin. HEK293T cells with active or epigenetically silenced *CD81* loci, were treated with the indicated ABE:gRNA and CBE:gRNA complexes designed for installing A > G and C > T substitutions, respectively, within their respective editing windows.

Total base edits within the quantification window and intended base edits within each editing window are plotted (top and bottom graphs, respectively). (**B**) Quantification of base-editing byproducts at open and closed chromatin. Base-editing byproducts corresponding to base edits inside and outside editing windows or only outside these windows are plotted as magenta and orange bar graphs, respectively. Base-editing byproducts corresponding to unintended substitutions and composite edits consisting of intended and unintended substitutions are plotted as grey and black bar graphs. Base editing events were measured through deep sequencing analyses (50,000 paired-end reads). Significances were determined via two-tailed Student's *t* tests with bars and error bars corresponding to mean ± s.d., respectively (n=3 biological replicates). $P > 0.05$ considered non-significant (ns).

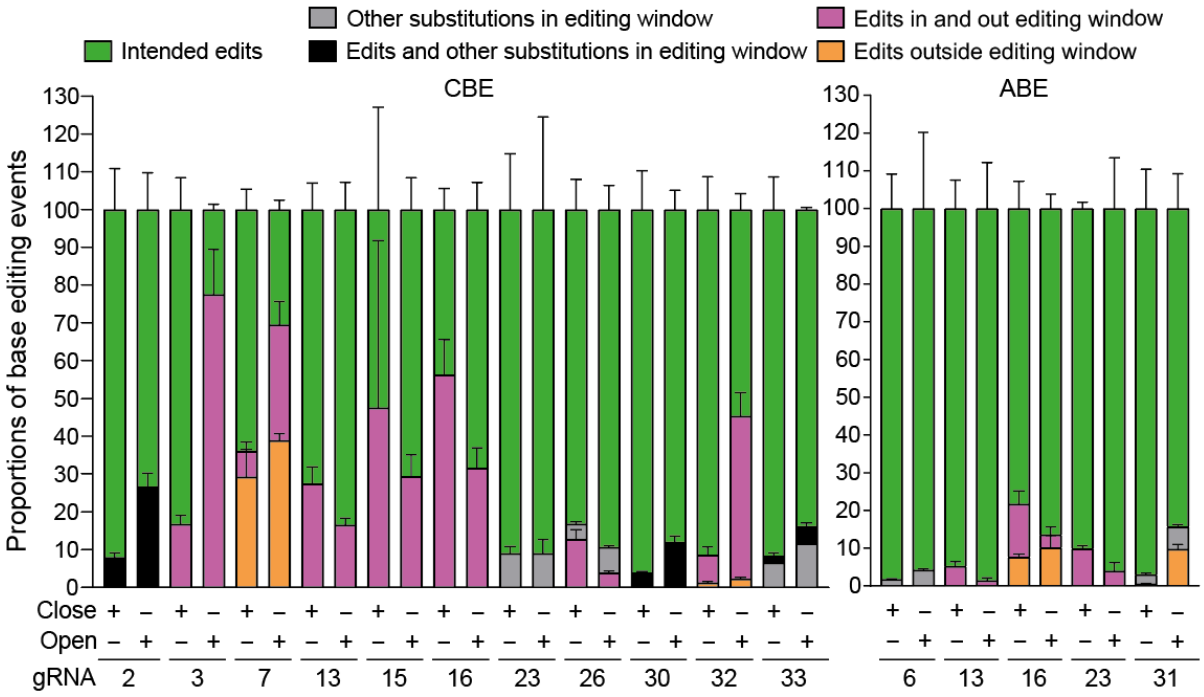

Supplementary Figure S9. Proportions of base editing events generated by CBE and ABE complexes. Relative frequencies of the different types of base editing events resulting from CBE and ABE complexes leading to significant differences in the amounts of byproducts at open versus closed chromatin (plotted from Figure 7 datasets).

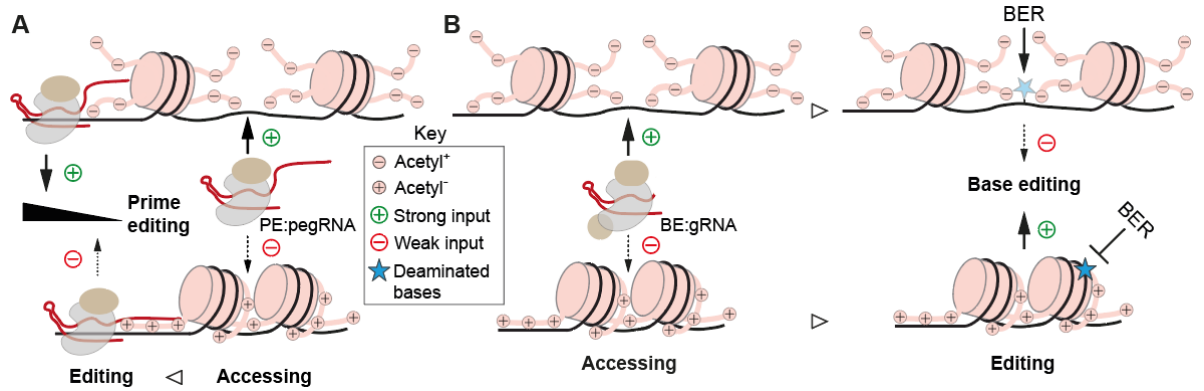

Supplementary Figure S10. Working models for the differential impact of chromatin organization on DSB-free gene editing tools. (**A**) Prime editing in open versus closed chromatin. PE:gRNA complexes access less frequently DNA in heterochromatin than euchromatin. Upon accessing heterochromatic target sites the 3'-ended extended portions of pegRNAs (i.e., PBS and RT templates) of prime editors locally interact with positively charged histone tails resulting in their trapping and consequent prime editing inhibition. Conversely, upon accessing euchromatic target sites these extended portions of pegRNAs are less likely to interact with acetylated negatively charged histone tails, resulting in their availability for DNA flap hybridization and reverse transcription. (**B**) base editing in open versus closed chromatin. As PE:gRNA complexes, BE:gRNA complexes access less frequently DNA in heterochromatin than in euchromatin. Upon accessing heterochromatic target sites, BE:gRNA complexes induce *in situ* deamination (stars). When compared to deaminated bases in euchromatin (light cyan star), deaminated bases in heterochromatin (dark cyan star) are more protected from reversion through base excision repair (BER) and, as a result, are more likely to remain a substrate for the downstream base editing processes. The postulated interactions (inputs) involving CRISPR complex accessibility to alternate chromatin conformations and local favouring or disfavouring of reverse transcriptase and deaminase activities results in a net negative or positive DNA editing output. Representative relative outputs of the herein investigated DSB-free DNA editing platforms in terms of chromatin impact indexes are as follows: PE:pegRNA > BE:gRNA.

SUPPLEMENTARY TABLES

Supplementary Table S1. Oligonucleotides used for gRNA assembly.

Plasmid name	Code	Oligonucleotide sequence (5' → 3')
AM51_pU6.gRNA$^{I\text{-}SceI.1}$	#25	ACCGGTGAGCTCTTATTTGCGTAGCTAGCTGAC
	#26	AAACGTCAGCTAGCTACGCAAATAAGAGCTCAC
BF23_pU6.opt-gRNA$^{eGFP.2}$ and AV59_pU6.gRNA$^{eGFP.2}$	#161	ACCGTCGCCCTCGAACTTCACCT
	#162	AAACAGGTGAAGTTCGAGGGCGA
BA21_pU6.opt-gRNA$^{eGFP.3}$	#163	ACCGTAGGTCAGGGTGGTCACGA
	#164	AAACTCGTGACCACCCTGACCTA
AW18_pU6.opt-gRNA$^{eGFP.5}$	#171	ACCGCGAGGGCGATGCCACCTA
	#172	AAACTAGGTGGCATCGCCCTCG
AW20_pU6.gRNA$^{eGFP.6}$	#173	ACCGGCGAGGGCGATGCCACCTA
	#174	AAACTAGGTGGCATCGCCCTCGC
AW22_pU6.gRNA$^{eGFP.7}$	#175	ACCGACCAGGATGGGCACCACCC
	#176	AAACGGGTGGTGCCCATCCTGGT
AW31_pU6.opt-gRNA$^{eGFP.9}$	#183	ACCGCGAGGAGCTGTTCACCG
	#184	AAACCGGTGAACAGCTCCTCG
AW46_pU6.opt-gRNA$^{eGFP.13}$	#195	ACCGGGCGAGGAGCTGTTCACCG
	#196	AAACCGGTGAACAGCTCCTCGCC
AX27_pU6.gRNA$^{eGFP.15.c}$	#199	ACCGATGCCGTTCTTCTGCTTGT
	#200	AAACACAAGCAGAAGAACGGCAT
AZ43_pU6.opt-gRNA$^{eGFP.16}$ and AX03_pU6.gRNA$^{eGFP.16}$	#203	ACCGCTCGTGACCACCCTGACCTA
	#204	AAACTAGGTCAGGGTGGTCACGAG
AB69_pU6.opt-gRNA$^{eGFP.23}$	#377	ACCGCAAGCAGAAGAACGGCATCA
	#378	AAACTGATGCCGTTCTTCTGCTTG
AM28_pU6.opt-gRNA$^{eGFP.25}$	#389	ACCGGACCATGGTGAGCAAGGGCG
	#390	AAACCGCCCTTGCTCACCATGGTC
AM31_pU6.opt-gRNA$^{eGFP.26}$	#395	ACCGGCTCACCATGGTGGCGAC
	#396	AAACGTCGCCACCATGGTGAGC
AK65_pU6.opt-gRNA$^{eGFP.29}$	#521	ACCGATGCCCTTCAGCTCGATG
	#522	AAACCATCGAGCTGAAGGGCAT
AK66_pU6.opt-gRNA$^{eGFP.30}$	#523	ACCGCCGTCGTCCTTGAAGAAGA
	#524	AAACTCTTCTTCAAGGACGACGG
AF69_pU6.opt-gRNA$^{eGFP.31}$	#429	ACCGCACCATGGTGAGCAAGGGCG
	#430	AAACCGCCCTTGCTCACCATGGTG
BF50_pU6.opt-gRNA$^{eGFP.32}$	#691	ACCGGCCGTAGGTCAGGGTGGTCACG
	#692	AAACCGTGACCACCCTGACCTACGGC
BH40_pU6.opt-gRNA$^{eGFP.33}$	#705	ACCGTTGCTCACCATGGTGGCGAC
	#706	AAACGTCGCCACCATGGTGAGCAA
X63_pU6.opt-gRNA$^{CD81.1}$.MCS	#722	ACCGAGAGCGAGCGCGCAACGG
	#723	AAACCCGTTGCGCGCTCGCTCT
X68_pU6.opt-gRNA$^{CD81.2}$.MCS	#724	ACCGGCCTGGCAGGATGCGCGG
	#725	AAACCCGCGCATCCTGCCAGGC
BG30_pU6.opt-gRNA$^{CD81.5}$	#740	ACCGCGCACCCATCACCACCACAG
	#741	AAACCTGTGGTGGTGATGGGTGCG
BG31_pU6.opt-gRNA$^{CD81.6}$	#742	ACCGAAGCAGCAGTCCGGAATCCG
	#743	AAACCGGATTCCGGACTGCTGCTT
BG32_pU6.opt-gRNA$^{CD81.7}$	#744	ACCGCTCATGGGGGCGGGGCGCC
	#745	AAACGGCGCCCCGCCCCCATGAG
BG33_pU6.opt-gRNA$^{CD81.8}$	#746	ACCGCGCAGATTGGAGAGTGAGCT
	#747	AAACAGCTCACTCTCCAATCTGCG
BH53_pU6.opt-gRNA$^{CD81.9}$	#809	ACCGGAGTTGATGCCACAGTGGT
	#810	AAACACCACTGTGGCATCAACTC
BH54_pU6.opt-gRNA$^{CD81.10}$	#811	ACCGATCTGGGAGGGCTCCCCAA
	#812	AAACTTGGGGAGCCCTCCCAGAT
BH55_pU6.opt-gRNA$^{CD81.11}$	#813	ACCGCCAAGGTGCTTGAGGGAGGG
	#814	AAACCCCTCCCTCAAGCACCTTGG
BH56_pU6.opt-gRNA$^{CD81.12}$	#815	ACCGCTGGGAGGGCTCCCCAAAGG
	#816	AAACCCTTTGGGGAGCCCTCCCAG
BH57_pU6.opt-gRNA$^{CD81.13}$	#817	ACCGCAGTACTTATAGGGCGCCG
	#818	AAACCGGCGCCCTATAAGTACTG

Supplementary Table S2. Oligonucleotides used for pegRNA assembly.

Plasmid names	Codes	Oligonucleotide sequences (5' → 3')
S77_pU6.PEgRNA^{TLR}	#623	CACCGTAACAGGGTAATGTCGAGGCGTTTT
	#624	CTCTAAAACGCCTCGACATTACCCTGTTAC
	#1424	AGAGCTAGAAATAGCAAGTTAAAATAAGGCTAGTCCGTTATCAACTTGAAAA AGTGGCACCGAGTCG
	#1425	GCACCGACTCGGTGCCACTTTTTCAAGTTGATAACGGACTAGCCTTATTTTA ACTTGCTATTTCTAG
	#1700	GTGCTTCAGCGTGTCCGGCCATCGACATTACCCTG
	#1701	AAAACAGGGTAATGTCGATGGCCGGACACGCTGAA
AG06_pU6.PEgRNA.2	#701	CACCGTCGCCCTCGAACTTCACCTGTTTT
	#702	CTCTAAAACAGGTGAAGTTCGAGGGCGAC
	#1424	AGAGCTAGAAATAGCAAGTTAAAATAAGGCTAGTCCGTTATCAACTTGAAAA AGTGGCACCGAGTCG
	#1425	GCACCGACTCGGTGCCACTTTTTCAAGTTGATAACGGACTAGCCTTATTTTA ACTTGCTATTTCTAG
	#1880	GTGCACCCGCGCCGAGGAATGAAGTTCGAGG
	#1881	AAAACCTCGAACTTCATTCCTCGGCGCGGGT
AG07_pU6.PEgRNA.34	#703	CACCGCTCGCCCTTGCTCACCATGGGTTTT
	#704	CTCTAAAACCCATGGTGAGCAAGGGCGAGC
	#1424	AGAGCTAGAAATAGCAAGTTAAAATAAGGCTAGTCCGTTATCAACTTGAAAA AGTGGCACCGAGTCG
	#1425	GCACCGACTCGGTGCCACTTTTTCAAGTTGATAACGGACTAGCCTTATTTTA ACTTGCTATTTCTAG
	#1882	GTGCACCGGTCGCCACCGTGGTGAGCAAG
	#1883	AAAACTTGCTCACCACGGTGGCGACCGGT
S70_pU6.PEgRNA.16	#617	CACCGCTCGTGACCACCCTGACCTAGTTTT
	#618	CTCTAAAACTAGGTCAGGGTGGTCACGAGC
	#1424	AGAGCTAGAAATAGCAAGTTAAAATAAGGCTAGTCCGTTATCAACTTGAAAA AGTGGCACCGAGTCG
	#1425	GCACCGACTCGGTGCCACTTTTTCAAGTTGATAACGGACTAGCCTTATTTTA ACTTGCTATTTCTAG
	#1418	GTGCAAGCACTGCACGCCGTGGGTCAGGGTGGTCA
	#1419	AAAATGACCACCCTGACCCACGGCGTGCAGTGCTT
BG26_pU6.PEgRNA$^{CD81.3}$	#748	CACCGCCCGGCCGCCCCTCAGCTAGTTTT
	#749	CTCTAAAACTAGCTGAGGGGCGGCCGGGC
	#1424	AGAGCTAGAAATAGCAAGTTAAAATAAGGCTAGTCCGTTATCAACTTGAAAA AGTGGCACCGAGTCG
	#1425	GCACCGACTCGGTGCCACTTTTTCAAGTTGATAACGGACTAGCCTTATTTTA ACTTGCTATTTCTAG
	#1949	GTGCCCCTCGTTAGCTGAGGGGCGG
	#1950	AAAACCGCCCCTCAGCTAACGAGGG
BG27_pU6.PEgRNA$^{CD81.4}$	#750	CACCGCATCAAGAGCCGCCGCCCCGTTTT
	#751	CTCTAAAACGGGGCGGCGGCTCTTGATGC
	#1424	AGAGCTAGAAATAGCAAGTTAAAATAAGGCTAGTCCGTTATCAACTTGAAAA AGTGGCACCGAGTCG
	#1425	GCACCGACTCGGTGCCACTTTTTCAAGTTGATAACGGACTAGCCTTATTTTA ACTTGCTATTTCTAG
	#1951	GTGCCCATCGAGGGGCGGCGG
	#1952	AAAACCGCCGCCCCTCGATGG
BH58_pU6.PEgRNA$^{CD81.9}$	#819	CACCGGAGTTGATGCCACAGTGGTGTTTT
	#820	CTCTAAAACACCACTGTGGCATCAACTCC
	#1424	AGAGCTAGAAATAGCAAGTTAAAATAAGGCTAGTCCGTTATCAACTTGAAAA AGTGGCACCGAGTCG
	#1425	GCACCGACTCGGTGCCACTTTTTCAAGTTGATAACGGACTAGCCTTATTTTA ACTTGCTATTTCTAG
	#2076	GTGCGCAAAGCGAACCACTGTGGCA
	#2077	AAAATGCCACAGTGGTTCGCTTTGC
BH59_pU6.PEgRNA$^{CD81.10}$	#821	CACCGATCTGGGAGGGCTCCCCAAGTTTT
	#822	CTCTAAAACTTGGGGAGCCCTCCCAGATC

	#1424	AGAGCTAGAAATAGCAAGTTAAAATAAGGCTAGTCCGTTATCAACTTGAAAAAGTGGCACCGAGTCG
	#1425	GCACCGACTCGGTGCCACTTTTTCAAGTTGATAACGGACTAGCCTTATTTTAACTTGCTATTTCTAG
	#2078	GTGCACCTCGTTTGGGGAGCCCT
	#2079	AAAAAGGGCTCCCCAAACGAGGT
BH61_pU6.PEgRNA[CD81.12]	#825	CACCGCTGGGAGGGCTCCCCAAAGGGTTTT
	#826	CTCTAAAACCCTTTGGGGAGCCCTCCCAGC
	#1424	AGAGCTAGAAATAGCAAGTTAAAATAAGGCTAGTCCGTTATCAACTTGAAAAAGTGGCACCGAGTCG
	#1425	GCACCGACTCGGTGCCACTTTTTCAAGTTGATAACGGACTAGCCTTATTTTAACTTGCTATTTCTAG
	#2082	GTGCCTCACGTCCTTTGGGGAGC
	#2083	AAAAGCTCCCCAAAGGACGTGAG
BH62_pU6.PEgRNA[CD81.13]	#827	CACCGCAGTACTTATAGGGCGCCGGTTTT
	#828	CTCTAAAACCGGCGCCCTATAAGTACTGC
	#1424	AGAGCTAGAAATAGCAAGTTAAAATAAGGCTAGTCCGTTATCAACTTGAAAAAGTGGCACCGAGTCG
	#1425	GCACCGACTCGGTGCCACTTTTTCAAGTTGATAACGGACTAGCCTTATTTTAACTTGCTATTTCTAG
	#2084	GTGCGGGACGGCGGCGCCCTATA
	#2085	AAAATATAGGGCGCCGCCGTCCC

Note: Green, grey and magenta oligonucleotides (sense and antisense) encode, respectively, sequence-specific spacers, pegRNA scaffolds and pegRNA 3' extensions with PBS and RT sequences.

Supplementary Table S3. Transfection scheme for assessing the activities of prime editors in HER.TLR[TetO.KRAB] cells (**Figure 2B, left panel**).

HER.TLR[TetO.KRAB] cells	4.0 ×10[5] cells per well of 24-well plates						
	2000 ng DNA and 9.60 µl PEI (1 mg ml[-1]) per well (medium replaced at 6 h post-transfection)						
Encoded products	Cas9[H840A]	PE2	pegRNA.TLR	gRNA.8	gRNA.16	gI-SceI	EGFP
Plasmid codes	AT79	S65	S77	AW24	AX03	AM51	C55
Construct length (bp)	9215	113	2305	3047	3047	3056	5771
1	1086		359				555
2		108	359				555
3	1086		359	119			555
4		108	359	119			555
5	1086		359		119		555
6		108	359		119		555
7	1086					359	555
8		108				359	555

Supplementary Table S4. Transfection scheme for testing the activities of prime editors in HER.TLR[KRAB] cells (**Figure 2B, right panel**).

HER.TLR[KRAB] cells	4.5 ×10[5] cells per well of 24-well plates						
	2000 ng DNA and 9.60 µl PEI (1 mg ml[-1]) per well (medium replaced at 6 h post-transfection)						
Encoded products	Cas9[H840A]	PE2	pegRNA.TLR	gRNA.8	gRNA.16	gI-SceI	EGFP
Plasmid codes	AT79	S65	S77	AW24	AX03	AM51	C55
Construct length	9215	11389	2305	3047	3047	3056	5771
1	1086		359				555
2		1086	359				555
3	1086		359	119			555
4		1086	359	119			555
5	1086		359		119		555
6		1086	359		119		555
7	1086					359	555
8		1086				359	555

Supplementary Table S5. Transfection scheme for determining target gene knockout frequencies induced by prime editors in HEK.EGFP$^{TetO.KRAB}$ cells (**Figure 2D**).

HEK.EGFP$^{TetO.KRAB}$ cells	2.5 ×10^5 cells per well of 24-well plates									
	1100 ng DNA and 4.61 µl PEI (1 mg ml^{-1}) per well (medium replaced at 6 h post-transfection)									
Encoded products	Cas9 ^{H840A}	PE2	pegRNA.2	gRNA. 21	gRNA. T2	pegRNA.34	gRNA. 6	gRNA. 8	gI-SceI	DsRed
Plasmid codes	AT79	S65	AG06	BB11	AT44	AG07	AW20	AW24	AM51	AM37
Construct	9215	11389	2306	3047	3974	2305	3046	3047	3056	4712
1	750								250	100
2		750	250							100
3		750	250	100						100
4		750	250		100					100
5		750				250				100
6		750				250	100			100
7		750				250		100		100
8		750							250	100

Supplementary Table S6. Transfection scheme for determining target gene knockout frequencies induced by prime editors in HEK.EGFP$^{TetO.KRAB}$ cells (**Figure 3B**).

HEK.EGFP$^{TetO.KRAB}$ cells	2.5 ×10^5 cells per well of 24-well plates						
	1100 ng DNA and 4.61 µl PEI (1 mg ml^{-1}) per well (medium replaced at 6 h post-transfection)						
Encoded products	Cas9^{H840A}	PE2	pegRNA.16	gRNA.2	gRNA.7	gI-SceI	DsRed
Plasmid codes	AT79	S65	S70	AV59	AW22	AM51	AM37
Construct length (bp)	9215	11389	2311	3047	3047	3056	4712
1		750	250			250	100
2	750		250	100			100
3		750	250	100			100
4	750		250		100		100
5		750			100		100
6	750					250	100
7		750				250	100

Supplementary Table S7. Transfection scheme for assessing the impact of chromatin conformations on the performance of gRNAs and pegRNAs in HER.TLR$^{TetO.KRAB}$ cells (**Figure 4A**).

HER.TLR$^{TetO.KRAB}$ cells	4.0 ×10^5 cells per well of 24-well plates			
	2000 ng DNA and 9.60 µl PEI (1 mg ml^{-1}) per well (medium replaced at 6 h post-transfection)			
Encoded products	Cas9	pegRNA.TLR	gRNA.TLR	EGFP
Plasmid codes	AV62	S77	AW24	C55
Construct length (bp)	9215	2305	3047	5771
1	1086	359		555
2	1086		359	555

Supplementary Table S8. Transfection scheme for testing the impact of chromatin conformations on the performance of gRNAs and pegRNAs in HER.TLR^{KRAB} cells (**Figure 4B**).

HER.TLR^{KRAB} cells	4.5 ×10^5 cells per well of 24-well plates			
	2000 ng DNA and 9.60 µl PEI (1 mg ml^{-1}) per well (medium replaced at 6 h post-transfection)			
Encoded products	Cas9	pegRNA.TLR	gRNA.TLR	EGFP
Plasmid codes	AV62	S77	AW24	C55
Construct length (bp)	9215	2305	3047	5771
1	1086	359		555
2	1086		359	555

Supplementary Table S9. Transfection scheme for assessing the impact of chromatin conformations on the performance of gRNAs and pegRNAs in HEK.EGFP$^{TetO.KRAB}$ cells (**Figure 4C**).

HEK.EGFP$^{TetO.KRAB}$ cells	2.5 ×10^5 cells per well of 24-well plates					
	1000 ng DNA and 4.61 µl PEI (1 mg ml^{-1}) per well (medium replaced at 6 h post-transfection)					
Encoded products	Cas9	pegRNA.16	gRNA.16	pegRNA.2	gRNA.2	DsRed
Plasmid codes	AV62	S70	AX03	AG06	AV59	AM37
Construct length (bp)	9215	2311	3047	2306	3047	4712

1	750	250				100
2	750		250			100
3	750			250		100
4	750				250	100

Supplementary Table S10. Transfection scheme for inducing closed chromatin remodeling at *CD81* loci in HEK293T cells. (**Supplementary Figure S4**).

HEK293T cells	2.0 ×10^5 cells per well of 24-well plates			
	1200 ng DNA and 5.27 µl PEI (1 mg ml^{-1}) per well (medium replaced at 6 h post-transfection)			
Encoded products	CRISPRoff v2.1	gRNA.CD81.1	gRNA.CD81.2	DsRed
Plasmid codes	W57	X63	X68	AM37
Construct length (bp)	11885	2311	3047	4712
1	947.3	252.7		
2	947.3		252.7	
3	782.5	208.8	208.8	
4	947.3			252.7
5				1200

Supplementary Table S11. Transfection scheme for assessing the activities of prime editors at *CD81* loci in open and closed chromatin in HEK293T cells (**Figure 5F**).

HEK293T cells (CD81-negative or CD81-positive)	2.5 ×10^5 cells per well of 24-well plates						
	1100 ng DNA and 4.61 µl PEI (1 mg ml^{-1}) per well (medium replaced at 6 h post-transfection)						
Encoded products	PE2	pegCD81.3	pegCD81.4	gCD81.5	gCD81.6	gCD81.7	gCD81.8
Plasmid codes	S65	BG26	BG27	BG30	BG31	BG32	BG33
Construct length (bp)	11389	2300	2296	3057	3057	3056	3057
1	750	250					
2	750	250		100			
3	750	250			100		
4	750	250				100	
5	750		250				
6	750		250				100

HEK293T cells (CD81-negative or CD81-positive)	2.0 ×10^5 cells per well of 24-well plates				
	1100 ng DNA and 4.61 µl PEI (1 mg ml^{-1}) per well (medium replaced at 6 h post-transfection)				
Encoded products	PE2	pegCD81.9	pegCD81.10	gCD81.12	gCD81.13
Plasmid codes	S65	BH53	BH54	BH56	3172
Construct length (bp)	11389	3172	3172	3173	3057
1	915	250			
2	750	250		100	
3	750	250			100
4	750	250			
5	750		250		
6	750		250		

Supplementary Table S12. Transfection scheme for determining editing frequencies induced by the adenine base editor ABEmax in HEK.EGFP$^{TetO.KRAB}$ cells (**Figure 6A**).

HEK.EGFP$^{TetO.KRAB}$ cells	2.0 ×10^5 cells per well of 24-well plates							
	750 ng DNA and 3.29 µl PEI (1 mg ml^{-1}) per well (medium replaced at 6 h post-transfection)							
Encoded products	Cas9	ABEmax	gRNA.2	gRNA.16	gRNA.31	gRNA.32	gI-SceI	DsRed
Plasmid codes	AV62	BD09	BF23	AZ43	AF69	BF50	AM51	AM37
Construct length (bp)	9215	10522	3172	3048	3046	3047	3056	4712
1	418.0			138.2				193.8
2		431.0					125.2	193.8
3		427.4	128.8					193.8
4		431.3		124.9				193.8
5		431.3			124.9			193.8
6		431.3				124.9		193.8

Supplementary Table S13. Transfection scheme for determining editing frequencies induced by the cytidine base editor coBE3-2NLS in HEK.EGFP$^{TetO.KRAB}$ cells (**Figure 6A**).

HEK.EGFP$^{TetO.KRAB}$ cells	2.0 ×10^5 cells per well of 24-well plates								
	750 ng DNA and 3.29 µl PEI (1 mg ml^{-1}) per well (medium replaced at 6 h post-transfection)								
Encoded products	Cas9	coBE3-2NLS	gRNA.2	gRNA. 16	gRNA. 26	gRNA. 29	gRNA. 30	gI-SceI	DsRed
Plasmid codes	AV62	BC58	BF23	AZ43	AM31	AK65	AK66	AM51	AM37
Construct	9215	10870	3172	3048	3055	3055	3056	3056	4712
1	417.6			138.6					193.8
2		434.1						122.1	193.8
3		430.6	125.6						193.8
4		434.5							193.8
5		434.1		122.1					193.8
6		434.2			122				193.8
7		434.2				122			193.8
8		434.1					122.1		193.8

Supplementary Table S14. Transfection scheme for determining editing frequencies induced by the adenine base editor ABEmax in HEK.EGFP$^{TetO.KRAB}$ cells (**Figure 7**).

HEK.EGFP$^{TetO.KRAB}$ cells	2.0 ×10^5 cells per well of 24-well plates								
	1100 ng DNA and 4.61 µl PEI (1 mg ml^{-1}) per well (medium replaced at 6 h post-transfection)								
Encoded products	ABEmax	gRNA.	gRNA.	gRNA.	gRNA.	gRNA.	gRNA.	gRNA.	DsRed
Plasmid codes	BD09	BA21	AW18	AW20	AW22	AW31	AW46	AZ43	AM37
Construct length (bp)	10522	3056	3045	3046	3046	3044	3046	3057	4712
1	682.0	198.0							220.0
2	682.0		198.0						220.0
3	682.0			198.0					220.0
4	682.0				198.0				220.0
5	682.0					198.0			220.0
6	682.0						198.0		220.0
7	682.0							198.0	220.0

Encoded products	ABEmax	gRNA.	gRNA.	gRNA.	gRNA.	gRNA.	gRNA.	gI-SceI	DsRed
Plasmid codes	BD09	AB69	AM28	AM31	AF69	BF50	BH40	AM51	AM37
Construct length (bp)	10522	3057	3057	3055	3057	3157	3173	3056	4712
8	682.0	198.0							220.0
9	682.0		198.0						220.0
10	682.0			198.0					220.0
11	682.0				198.0				220.0
12	682.0					198.0			220.0
13	682.0						198.0		220.0
14	682.0							198.0	220.0

Supplementary Table S15. Transfection scheme for determining editing frequencies induced by the cytidine base editor coBE3-2NLS in HEK.EGFP$^{TetO.KRAB}$ cells (**Figure 7**).

HEK.EGFP$^{TetO.KRAB}$ cells	2.0 ×10^5 cells per well of 24-well plates									
	1100 ng DNA and 4.61 µl PEI (1 mg ml^{-1}) per well (medium replaced at 6 h post-transfection)									
Encoded products	coBE3-2NLS	gRNA. 2	gRNA.3	gRNA. 5	gRNA. 6	gRNA. 7	gRNA. 9	gRNA. 13	gRNA. 15C	DsRed
Plasmid codes	BC58	BF23	BA21	AW18	AW20	AW22	AW31	AW46	AX27	AM37
Construct length (bp)	10870	3172	3056	3045	3046	3046	3044	3046	3046	4712
1	687.0	193.0								220.0
2	687.0		193.0							220.0
3	687.0			193.0						220.0
4	687.0				193.0					220.0
5	687.0					193.0				220.0
6	687.0						193.0			220.0

7	687.0							193.0		220.0
8	687.0								193.0	220.0
Encoded	coBE3-	gRNA.	gRNA.	gRNA.	gRNA.	gRNA.	gRNA.	gRNA.	gI-SceI	DsRed
Plasmid codes	BC58	AZ43	AB69	AM28	AM31	AF69	BF50	BH40	AM51	AM37
Construct length	10870	3057	3057	3057	3055	3057	3157	3173	3056	4712
9	687.0	193.0								220.0
10	687.0		193.0							220.0
11	687.0			193.0						220.0
12	687.0				193.0					220.0
13	687.0					193.0				220.0
14	687.0						193.0			220.0
15	687.0							193.0		220.0
16	687.0								193.0	220.0

Supplementary Table S16. Transfection scheme for assessing the activities of both base editors at *CD81* loci in open and closed chromatin in HEK293T cells (**Figure 8** and **Supplementary Figure S6**).

HEK293T cells (CD81-negative or CD81-positive)	2.0 ×10^5 cells per well of 24-well plates 1000 ng DNA and 4.39 μl PEI (1 mg ml^{-1}) per well (medium replaced at 6 h post-transfection)							
Encoded products	ABEmax	coBE3-2NLS	gCD81.9	gCD81.10	gCD81.11	gCD81.12	gCD81.13	gI-SceI
Plasmid codes	BD09	BC58	BH53	BH54	BH55	BH56	BH57	AM51
Construct length	10522	10870	3172	3173	3173	3173	3172	3056
1	845.0		255.0					
2	845.0				255.0			
3	845.0					255.0		
4	845.0						255.0	
5	845.0							255.0
6		852.0	248.0					
7		852.0		248.0				
8		852.0			248.0			
9		852.0				248.0		
10		852.0					248.0	
11		852.0						248.0

Supplementary Table S17. Composition of mixtures used for qPCR amplification.

Targets	**Primer codes**	**Primers (5' → 3')**	**SYBR Green Master mix**	**Primers (μM)**	**Amplicons size (bp)**
CD81 (qPCR)	#1958	CTGCTTTGACCACCTCAGTGCT	1×	0.2	798
	#1959	TGGCAGCAATGCCGATGAGGTA			
GAPDH (qPCR)	#119	AGCCACATCGCTCAGACACC	1×	0.2	302
	#120	GTACTCAGCGCCAGCATCG			
CD81 b (ChIP-qPCR)	#2004	ATCAACTCCTTCAGGAAGCCC	1×	0.2	113
	#2005	CCGGGAGAACAACCCATTCC			
CD81 c (ChIP-qPCR)	#2006	CAGCAATTCTCCCCTTCCGT	1×	0.2	120
	#2007	TTGCTCACATTGCTCTCCGG			
GAPDH a (ChIP-qPCR)	#1998	CGCGCCCCCGGTTTCTAT	1×	0.2	80
	#1999	GATGCGGCTGACTGTCGAA			
GAPDH b (ChIP-qPCR)	#2000	TACTAGCGGTTTTACGGGCG	1×	0.2	166
	#2001	TCGAACAGGAGGAGCAGAGAGCGA			
GAPDH c (ChIP-qPCR)	#2024	TAGGCGCTCACTGTTCTCTC	1×	0.2	82
	#2025	CGTTGACTCCGACCTTCAC			
ACTB (ChIP-qPCR)	#2020	AACTCTCCCTCCTCCTCTTCC	1×	0.2	69
	#2021	CCTCTCCCCTCCTTTTGC			
ZNF184 (ChIP-qPCR)	#2022	TTGGGAATATGAAGGCAGTT	1×	0.2	60
	#2023	TCCTTTGGCAGTGTCTGTTG			

Supplementary Table S18. Thermocycler program used in qPCR amplification.

Steps	**Temperatures**	**Times**
Initial denaturation	95.0 ℃	5 min
Denaturation	95.0 ℃	10 sec

Annealing	60.0 ℃	30 sec
Elongation		
Plate read		
Cycles (Go to step 2)	45	
Melt curve analysis	65.0 ℃ to 95.0 ℃ (increase in 0.5 ℃ increments with a hold time of 5 sec	
Plate read		

Supplementary Table S19. Gene-specific primer sequences and concentrations used in the NGS analyses.

Target	Primer code	Primers (5' → 3') / final concentrations (μM)
eGFP	#1791	GATGTGTATAAGAGACAGGCACGACTTCTTCAAGTCCG / 0.5
	#1792	CGTGTGCTCTTCCGATCTAGTTCACCTTGATGCCGTTC / 0.5
eGFP	#1884	GATGTGTATAAGAGACAGATGCCACCTACGGCAAGCTG / 0.5
	#1885	CGTGTGCTCTTCCGATCTCCTCCTTGAAGTCGATGCCC / 0.5
eGFP	#1916	GATGTGTATAAGAGACAGCGATCACGAGACTAGCCTCG / 0.5
	#1917	CGTGTGCTCTTCCGATCTTAGGTCAGGGTGGTCACGAG / 0.5
eGFP	#2087	GATGTGTATAAGAGACAGCATCGACTTCAAGGAGGACGG / 0.5
	#2088	CGTGTGCTCTTCCGATCTGGGTGTTCTGCTGGTAGTGG / 0.5
CD81	#1987	GATGTGTATAAGAGACAGTTTCGGGGCCTCTGTGCTCG / 0.5
	#1988	CGTGTGCTCTTCCGATCTACCTCCGGCAAAGTGTGCGC / 0.5
CD81	#1989	GATGTGTATAAGAGACAGGGATTCCGGACTGCTGCTTCGC / 0.5
	#1990	CGTGTGCTCTTCCGATCTACCCCAGCTTCTGGGCCATC / 0.5
CD81	#2095	GATGTGTATAAGAGACAGGGTGCAGCGACCCCATACCCC / 0.5
	#2096	CGTGTGCTCTTCCGATCTGCCTGGCAGGATGCGCGGTG / 0.5

Supplementary Table S20. PCR cycling parameters used in the NGS analyses.

Target	Initial denaturation	Denaturation	Annealing	Elongation	Cycles	Final elongation
eGFP (1791+1792) (gene-specific PCR)	98 ℃	98 ℃	61.1 ℃	72 ℃	35	72 ℃
	30 sec	10 sec	10 sec	10 sec		5 min
eGFP (1884+1885) (gene-specific PCR)	98 ℃	98 ℃	70.5 ℃	72 ℃	35	72 ℃
	30 sec	10 sec	10 sec	10 sec		5 min
eGFP (1916+1917) (gene-specific PCR)	98 ℃	98 ℃	67.6 ℃	72 ℃	35	72 ℃
	30 sec	10 sec	10 sec	10 sec		5 min
eGFP (2087+2088) (gene-specific PCR)	98 ℃	98 ℃	67.0 ℃	72 ℃	35	72 ℃
	5 min	10 sec	10 sec	10 sec		5 min
CD81 (1987+1988) (gene-specific PCR)	98 ℃	98 ℃	67.6 ℃	72 ℃	35	72 ℃
	30 sec	10 sec	10 sec	10 sec		5 min
CD81 (1989+1990) (gene-specific PCR)	98 ℃	98 ℃	71.6 ℃	72 ℃	35	72 ℃
	30 sec	10 sec	10 sec	10 sec		3 min
CD81 (2095+2096) (gene-specific PCR)	98 ℃	98 ℃	71.0 ℃	72 ℃	35	72 ℃
	5 min	10 sec	10 sec	10 sec		5 min
Barcode PCR	98 ℃	98 ℃	62.0 ℃	72 ℃	10	72 ℃
	30 sec	10 sec	10 sec	10 sec		3 min

Supplementary Table S21. Composition of PCR mixtures used in gene-specific amplifications for NGS analyses.

Component	Volume	Final Concentration
5× Phusion HF Buffer	4 μl	1×
dNTPs (2.5 mM each)	1.6 μl	0.2 mM (each)
PCR Grade Water	10.7 μl	-
Forward primer (10 μM)	1 μl	0.5 μM
Reverse primer (10 μM)	1 μl	0.5 μM
gDNA	1.5 μl	-
Phusion DNA Polymerase (2 U/μl)	0.2 μl	0.02 U/μl
Total reaction volume	20 μl	-

Supplementary Table S22. Barcoded PCR primers used in the NGS analyses.

Primer	Primers (5' → 3') / final concentrations (0.25 µM)
Fun-i501	AATGATACGGCGACCACCGAGATCTACACTAGATCGCTCGTCGGCAGCGTCAGATGTGTATAAGAGACA
Fun-i502	AATGATACGGCGACCACCGAGATCTACACCTCTCTATTCGTCGGCAGCGTCAGATGTGTATAAGAGACAG
Fun-i503	AATGATACGGCGACCACCGAGATCTACACTATCCTCTTCGTCGGCAGCGTCAGATGTGTATAAGAGACAG
Fun-i504	AATGATACGGCGACCACCGAGATCTACACAGAGTAGATCGTCGGCAGCGTCAGATGTGTATAAGAGACA
Fun-i505	AATGATACGGCGACCACCGAGATCTACACGTAAGGAGTCGTCGGCAGCGTCAGATGTGTATAAGAGACA
Fun-i506	AATGATACGGCGACCACCGAGATCTACACACTGCATATCGTCGGCAGCGTCAGATGTGTATAAGAGACA
Fun-i507	AATGATACGGCGACCACCGAGATCTACACAAGGAGTATCGTCGGCAGCGTCAGATGTGTATAAGAGACA
Fun-i508	AATGATACGGCGACCACCGAGATCTACACCTAAGCCTTCGTCGGCAGCGTCAGATGTGTATAAGAGACA
Fun-i517	AATGATACGGCGACCACCGAGATCTACACGCGTAAGATCGTCGGCAGCGTCAGATGTGTATAAGAGACA
Fun-i501D	AATGATACGGCGACCACCGAGATCTACACTATAGCCTTCGTCGGCAGCGTCAGATGTGTATAAGAGACA
Fun-i502D	AATGATACGGCGACCACCGAGATCTACACATAGAGGCTCGTCGGCAGCGTCAGATGTGTATAAGAGACA
Fun-i503D	AATGATACGGCGACCACCGAGATCTACACCCTATCCTTCGTCGGCAGCGTCAGATGTGTATAAGAGACA
Fun-i504D	AATGATACGGCGACCACCGAGATCTACACAGAGTAGATCGTCGGCAGCGTCAGATGTGTATAAGAGACA
Fun-i505D	AATGATACGGCGACCACCGAGATCTACACGTAAGGAGTCGTCGGCAGCGTCAGATGTGTATAAGAGACA
Fun-i506D	AATGATACGGCGACCACCGAGATCTACACACTGCATATCGTCGGCAGCGTCAGATGTGTATAAGAGACA
Fun-i507D	AATGATACGGCGACCACCGAGATCTACACAAGGAGTATCGTCGGCAGCGTCAGATGTGTATAAGAGACA
Fun-i701	CAAGCAGAAGACGGCATACGAGATTCGCCTTAGTGACTGGAGTTCAGACGTGTGCTCTTCCGATCT
Fun-i702	CAAGCAGAAGACGGCATACGAGATCTAGTACGGTGACTGGAGTTCAGACGTGTGCTCTTCCGATCT
Fun-i703	CAAGCAGAAGACGGCATACGAGATTTCTGCCTGTGACTGGAGTTCAGACGTGTGCTCTTCCGATCT
Fun-i704	CAAGCAGAAGACGGCATACGAGATGCTCAGGAGTGACTGGAGTTCAGACGTGTGCTCTTCCGATCT
Fun-i705	CAAGCAGAAGACGGCATACGAGATAGGAGTCCGTGACTGGAGTTCAGACGTGTGCTCTTCCGATCT
Fun-i706	CAAGCAGAAGACGGCATACGAGATCATGCCTAGTGACTGGAGTTCAGACGTGTGCTCTTCCGATCT
Fun-i707	CAAGCAGAAGACGGCATACGAGATGTAGAGAGGTGACTGGAGTTCAGACGTGTGCTCTTCCGATCT
Fun-i708	CAAGCAGAAGACGGCATACGAGATCCTCTCTGGTGACTGGAGTTCAGACGTGTGCTCTTCCGATCT
Fun-i709	CAAGCAGAAGACGGCATACGAGATAGCGTAGCGTGACTGGAGTTCAGACGTGTGCTCTTCCGATCT
Fun-i710	CAAGCAGAAGACGGCATACGAGATCAGCCTCGGTGACTGGAGTTCAGACGTGTGCTCTTCCGATCT
Fun-i711	CAAGCAGAAGACGGCATACGAGATTGCCTCTTGTGACTGGAGTTCAGACGTGTGCTCTTCCGATCT
Fun-i712	CAAGCAGAAGACGGCATACGAGATTCCTCTACGTGACTGGAGTTCAGACGTGTGCTCTTCCGATCT

Supplementary Table S23. Composition of PCR mixtures for barcoded PCR amplification in the NGS analyses.

Component	**Volume**	**Final Concentration**
5× Phusion HF Buffer	4 µl	1×
dNTPs (2.5 mM each)	1.2 µl	0.15 mM (each)
PCR Grade Water	11.6 µl	-
Index primer p5-XX (5 µM)	1 µl	0.25 µM
Index primer p7-XX (5 µM)	1 µl	0.25 µM
Purified PCR product	1 µl	-
Phusion DNA Polymerase (2 U/µl)	0.2 µl	0.02 U/µl
Total reaction volume	20 µl	-